gin here »

REACTION MECHANISM AND SPECTROSCOPY OF TRANSFER REACTIONS INDUCED BY HEAVY IONS

M.-C. Lemaire

Département de Physique Nucléaire
CEN Saclay, BP 2, 91190 Gif-sur-Yvette, France

INTRODUCTION

In these last years an enormous amount of experimental and theoretical works has been devoted to the study of heavy ion induced few nucleon transfer reactions. To understand the mechanism of these reactions a great number of one nucleon transfer data have been measured and analyzed. These data have well established the basic features of heavy ion reaction dynamics [1-2] : i) a strong dependence of the cross-section on Q value and angular momentum matching conditions; ii) the evolution of the angular distributions from bell shapes to forward peaked cross-sections with increasing incident energies.

The validity of direct reaction theory to heavy ion few nucleon transfer reactions has been reviewed by K.S. Low [3] last year at the Caen Conference. He has shown that most features of the single nucleon transfer reactions can be described in the framework of either the Distorted Wave Born Approximation (DWBA) or Coupled Channel Born Approximation (CCBA). Consequently in the present talk, I shall confine the discussion to the study of two and four nucleon transfer reactions which can be used as probe of nuclear structure in addition to the investigation of the reaction mechanism.

The analysis of the transfer data by means of DWBA or CCBA codes requires the use of an optical potential to calculate the incoming and outgoing distorted waves. Such a determination of an optical potential has initiated many measurements of heavy ion elastic and inelastic angular distributions. So I shall begin this talk with a discussion on the specific features displayed by these data, pointing out their physical origin from semi-classical calculations.

I. THE ELASTIC SCATTERING

Despite a large amount of effort developed by both theorists and experimentalists on the determination of an optical model potential describing heavy ion interaction, the characteristics of such a potential are not yet well established [4-5]. This is due to the fact that at low incident energies the elastic scattering data are only sensitive to a very small region of the extreme tail of the potential. Consequently a lot of ambiguities have been found between optical model parameter families able to reproduce the experimental angular distributions. In order to sample a broader region of the potential, elastic scattering data have been measured on a wide range of incident energies for the $^{16}O + ^{28}Si$ system [6,7]. The choice of these experimental data to illustrate heavy ion elastic scattering has been motivated by the following reasons :

a) They display most of the features observed in heavy ion elastic scattering data.

b) They have stimulated a lot of discussions on the properties of the optical potential which can reproduce the data [8].

c) Calculations of these angular distributions have been performed in the framework of the semi-classical formalism developed by J. Knoll and R. Schaeffer [9]. It shows that this model is a very powerful tool to investigate the physical origin of the observed angular distributions.

Conference on physics of medium-light nuclei.
Florence, Italy, 7-10 June 1977

CEA-CONF--4001

FR7800105

egin here »

Description of the data

The angular distributions are displayed on Fig.1. It shows that the cross-section is Rutherford at forward angles and exhibits an exponential decrease at backward angles. The angle where the cross-section deviates from Rutherford is moving to forward direction with increasing incident energy. At high incident energy the angular distributions have strong oscillations typical of a Fraunhofer diffraction pattern.

The optical potential ambiguities

These data have been initially fitted with a unique energy independent Wood-Saxon potential (V = 10 MeV, r_{ov} = 1.35, a_v = .618, W = 23.4, r_{ow} = 1.23, a_w = .552 [6]). Such potential is surface transparent and has a shallow real depth. Further investigations have been performed by G.R. Satchler [8] to know to what extent these measurements have really determined an optical potential. He found equally good fits to the data with either a folded real potential or even other Wood-Saxon optical potentials once the diffuseness of the imaginary part of the potential is allowed to increase with increasing incident energies. These potentials may be deep in the interior like the folded potential or shallow like the Wood-Saxon potential. As the potentials able to reproduce the Cramer's data exhibit different shapes at the nuclear surface, it has been concluded that the optical potential cannot be precisely determined even at the nuclear surface.

Finally, the angular distribution measurements of this $^{16}O + ^{28}Si$ elastic scattering have been extended to very backward angles [7]. As it can be seen from Fig.2, the corresponding cross-section exhibits strong oscillations whith a rise at backward angles. Such a behavior is very similar to that previously observed in the scattering of light nuclei such as $^{16}O + ^{12}C$ [10]. No optical model fit has yet been able to reproduce the data.

These difficulties encountered in the phenomenological description of the optical potential are reflected in the analysis of the transfer data as these latter might be sensitive to a radial region of the potential different from that important for elastic scattering [11,12].

Semi-classical description of the data [13]

Semi-classical calculations have been done for elastic scattering of ^{16}O on ^{28}Si in the framework of the CWKB formalism derived by J. Knoll and R. Schaeffer [9]. The advantage of their model over previous semi-classical calculations [14] is to allow the use of a complex potential so that both absorptive, refractive and diffractive effects could be taken into account simultaneously. As shown on Fig.3, the semi-classical calculations agree fairly well with the corresponding quantum mechanical calculations. An interesting aspect of the semi-classical treatment is that the cross-section can be formulated as a sum of few terms which can be associated to the classical trajectories displayed on Fig.4. The trajectory named CT^+ corresponds to the Coulomb trajectory, the NT^+ and NT^- are those deflected by the attractive part of the nuclear potential respectively to the positive and negative angles. IT is an inner trajectory which contributes only in case of a weak absorption or at high incident energy.

The DT^+ trajectory is just the continuation of the Coulomb trajectory. It is called DT^+ beyond the Coulomb rainbow because there the process corresponds to a diffraction by the edge of the nuclear potential leading to a scattering towards positive angles. The relative contributions of these trajectories to the cross-sections are displayed on Fig.5 and Fig.6.

At angles forward from the Coulomb rainbow only the Coulomb CT^+ and nuclear NT^+ trajectories contribute, their interference produces small oscillations above the Rutherford cross-section. Beyond the Coulomb rainbow the cross-section is just coming from the DT^+ trajectory at 33 MeV and 50 MeV as the IT contribution is negligible due to the strong absorption. At 215.2 MeV incident energy, the oscillations result from interference between the NT^- trajectory and the trajectories deflected to the positive angles $DT^+ + IT^+$. At this energy the contribution of the

gin here »» internal trajectory is not anymore negligible.

Previously, they have been two interpretations to the low energy angular distributions. One suggests that the exponential fall off is due to strong absorption [15], others describe it as resulting of the deflection of the trajectories towards small angles by the attractive real part of the nuclear force [14,16]. To distinguish the respective role played by the real and imaginary parts of the potential, calculations using the same CT^+, NT^+ and DT^+ trajectories have been performed for 1) the real part of the potential alone, 2) the imaginary part of the potential alone. At 50 and 215.2 MeV the diffraction by the edge of the real potential alone is quite close to the full calculation (Fig.7). At 33 MeV the calculation with the full potential lies between the calculations using W = 0 and V = 0 with a slight preference for the former.

These investigations show that the role of absorption is mainly to suppress the contribution of the internal trajectory, while the slope of the cross-section fall off is mainly determined by the real part of the optical potential.

II. THE INELASTIC SCATTERING DATA

Next to elastic scattering, the inelastic scattering is the simplest process taking place between two heavy ions. Fig.8 displays a typical inelastic scattering angular distribution for an incident energy which is about twice the Coulomb barrier [17]. Model calculations have been performed isolating the contributions of Coulomb inelastic excitation and nuclear inelastic excitation. They show [18] that the forward angle cross-section is due to Coulomb excitation. The nuclear inelastic excitation is bell shaped due to the shorter range of the nuclear interaction. In the region of the grazing angle where the elastic distribution displays a maximum above the Rutherford cross-section, there is a destructive interference due to the fact that Coulomb and nuclear interaction have opposite signs.

According to the semi-classical model developed by R. Malfiet [14] the forward angle oscillations have been interpreted as due to interference between the Coulomb trajectory (CT^+) and the trajectory deflected to the positive angles by the attractive part of the nuclear potential (NT^+). From the opposite signs of the Coulomb and nuclear inelastic excitations, the model predicts that the oscillations in the inelastic cross-section will be 180° out of phase with the elastic cross-section. This is independent of the multipolarity of the inelastic cross-section. Indication of such phase rule has been observed for the $^{16}O + ^{76}Ge$ data displayed on Fig.9.

Contributions of multistep processes have been found to be significant for many heavy ion inelastic cross-sections [19,20]. Recent measurements, performed at Brookhaven [21], revealed that a strong coupling to the inelastic states can strongly affect the elastic cross-section. Fig.10 shows that the elastic angular distribution of ^{18}O on ^{184}W exhibits a dramatic change from the usual Coulomb rainbow picture. The observation at forward angles of a cross-section smaller than the Rutherford value can be reproduced only with coupled channel calculations and has been found due to the strong Coulomb excitation of the first 2^+ state. This interpretation is consistent with the observation of a similar behavior in the $^{16}O + ^{184}W$ elastic scattering, and a less striking effect for the ^{12}C projectile.

Finally, the case of the inelastic excitation of the ^{18}O, 1.98 MeV 2^+ state is still puzzling. The angular distributions of such inelastic excitation have been measured on many target nuclei [22,17], but the position of the Coulomb-nuclear interference minimum cannot be reproduced neither by DWBA nor by coupled channel calculations (Fig.11). It has been suggested by K.S. Low [3] that sequential transfer via the (^{18}O, ^{17}O) one neutron transfer can be at the origin of such pattern. This hypothesis has not yet been checked.

III. THE TWO NUCLEON TRANSFER REACTIONS

The (^{16}O, ^{14}C) and (^{12}C, ^{10}Be) two proton transfer reactions have been investigated on a large number of target nuclei and on a wide range of incident energies [23,24,25]. Their study was mainly motivated by the fact that little data

gin here »

exist on the corresponding light ion reaction (^{3}He,n), due to the experimental difficulties encountered in the neutron detection. In contrast, standard telescope techniques have been successful in identifying ^{14}C and ^{10}Be from the other isotopes. The study of heavy ion two neutron transfer or pick-up reactions has been carried out only more recently as it requires time of flight or magnetic spectrometer techniques to identify the reaction products. In this section it will be discuss :

- The selectivity of these reactions compared to the analogous light ion induced reactions.
- The shapes of the angular distributions observed in direct transfer.
- The importance of two step processes where the transfer occurs via inelastic excitation of either the target or residual nuclei.
- The absolute cross-section problem.

A - The heavy ion reaction selectivity

The comparison of the (^{16}O, ^{14}C) spectra (Fig.12) measured at Argonne on ^{42}Ca and ^{48}Ca targets [25] to the (^{3}He,n) data is a good example of the relative selectivities of light and heavy ion induced reactions. Both the (^{16}O, ^{14}C) and (^{3}He,n) reactions weakly excite the 1.9 MeV 0^+ state in ^{44}Ti compared to the ^{44}Ti ground-state. In contrast the low lying 4^+ and 6^+ states of ^{50}Ti are strongly excited by the (^{16}O, ^{14}C) reaction while they are not observed in the (^{3}He,n) study.

Another example of strong selectivity of two nucleon transfer reaction is shown on Fig.13 for the ^{26}Mg(^{18}O, ^{16}O)^{28}Mg reaction measured at 50 MeV incident energy with the Orsay M.P [26]. This reaction populates individual states up to 10 MeV excitation energy. It has to be emphasized that the 7 states observed between 7 and 10.55 MeV excitation energy have never been reported before the present experiment. Spins of ^{28}Mg levels have been assigned only for levels below 5.7 MeV excitation energy either from (t,p) angular distributions [27] or by (t,pγ) angular correlations [28]. No spins are known for states lying at higher excitation energy. The ^{26}Mg(^{18}O, ^{16}O)^{28}Mg data exhibits a selectivity similar to that previously observed in the (t,p) experiment (except for the 1.47 MeV level).

As it is well known that heavy ion induced transfer cross-sections are strongly dependent on Q value and angular momentum matching conditions, DWBA calculations have been performed to know which are the spins favored in the excitation energy region presently studied. The results show that between 6 and 10 MeV excitation energy, the reaction dynamics favored the population of 2^+, 3^- and 4^+ states.

B - Angular distributions of direct transfer

At energies near the Coulomb barrier these reactions exhibit bell shaped angular distributions centered around the grazing angle and independent of the angular momentum transferred [23]. At energies well above the Coulomb barrier the angular distributions display pronounced forward oscillations, which under favorable kinematic conditions, can serve as indicators of the transferred angular momentum. A good example is given by the 56 MeV ^{48}Ca(^{16}O, ^{14}C) Argonne data [25] going to the 0^+, 2^+, 4^+ and 6^+ states of ^{50}Ti (Fig. 14). For L $\neq$ 0 transitions, the DWBA cross-section is an incoherent sum over the different magnetic substate contributions

$$\sum_{m=-L}^{m=+L} \left| \sum_{\ell_\gamma} \beta^{m}_{\ell_\gamma} P^{m}_{\ell_\gamma} (\cos\theta \right|^2$$

The oscillations and L dependence observed in the above example arise from a dominance of the $|m| = L$ contribution for well matched transitions. In the general case of non well matched transitions, the different magnetic substates have similar importance. As the contributions of odd and even magnetic substates are out of phase, it results a strong damping of the oscillations and lack of L dependence.

The angular distributions of the ^{26}Mg(^{18}O, ^{16}O)^{28}Mg reaction going the ground-state and first 2^+ excited state are displayed on Fig.15. it exhibits strong

gin here »

oscillations with a period of ≈ 7° which is characteristic of the grazing ℓ_g value ($\ell_g \approx 26$). At forward angles, these two angular distributions exhibit a slight difference as expected from DWBA calculations. Angular distributions of the other levels have been measured, and the investigation of the spin dependence of these angular distributions is underway.

C - Two step process

Two nucleon transfer reactions induced by heavy ions have been specially successful in pointing out the contribution of two step process (where the transfer is preceeding or following inelastic excitation). An important feature of these reactions is that at incident energies not too high above the Coulomb barrier the angular distribution of a two step transfer mechanism is strongly different from that of a one step direct transfer. Many examples have been reported in recent experimental data (see Table I). One of them measured at Saclay [29] is displayed on Fig.16. It corresponds to angular distributions of the ground, first 2^+ and first 3^- excited states of ^{74,76,73}Se isotopes populated by the (^{16}O, ^{14}C) reactions on Ge targets. The angular distributions to the ground and 3^- states are essentially bell shaped, whereas those from the 2^+ states vary from a bell shape in the case of ^{74}Se to a forward peaking pattern for ^{76}Se and ^{78}Se. Such shape changes between different final state angular distributions have been rather well described in the framework of CCBA formalism [29] including the 2^+ and 3^- inelastic excitation of the target and residual nuclei.

It has to be emphasized that two step contributions were also seen in (p,t) reactions. But in this light ion experiment the direct and indirect angular distributions differ only in the extreme forward region, making the existence of such process more difficult to establish from the data. In contrast for heavy ion reactions at properly chosen incident energies the shape difference is so well marked that an examination of the data is generally sufficient to discriminate between the two reaction mechanisms.

For the Ge(^{16}O, ^{14}C)Se reactions, the CCBA calculations have shown that the forward peaking of the ^{76}Se and ^{78}Se 2^+ state angular distributions results from a destructive interference between the direct and indirect transitions. In the case of the 3^- state, the two step processes have been found still rather significant, in spite of the fact that the $0^+ - 3^-$ coupling is rather weak in both the entrance and exit channels between the direct and indirect routes. As the interference is constructive the observed angular distributions are bell shaped.

Forward peaked angular distributions have also been observed for 2^+ states which were excited by purely two step transfer [30,31]. An example is given on Fig.17 for the ^{76}Ge(^{16}O, ^{18}O)^{74}Ge data measured at Brookhaven. In this case one cannot invoke a destructive interference between the direct and indirect contributions to explain the absence of grazing peak as the direct contribution is completely suppressed by the structure of these states. In fact for a purely two step process the transfer is associated with inelastic excitation produced either by nuclear or Coulomb interaction. As these two contributions have opposite signs an interference which is always destructive occurs in the region of the grazing angle.

Angular distributions of the ^{74}Ge(^{18}O, ^{16}O)^{76}Ge two neutron stripping reaction have been also measured. They are displayed on Fig.18. The angular distribution of the ^{76}Ge ground-state is identical to that of the ^{76}Ge(^{16}O, ^{18}O)^{74}Ge$_{g.s}$ transition as expected for time-reversed reactions. That of the ^{76}Ge 2^+_1 state exhibits a steep drop near the grazing angle followed by a plateau between 40° and 55°. The main features of such a peculiar shape are reproduced by a CCBA calculation. By this analysis we have been able to establish that the ^{76}Ge 2^+_1 angular distribution is resulting from an interference between the direct and indirect transitions. In addition, the ℓ distribution of the transfer cross-section shows that the interference between the direct and indirect routes is respectively destructive or constructive depending on the fact that two-step process is occurring via nuclear or Coulomb inelastic excitation [30].

It should be mentioned that the CCBA angular distributions displayed on Fig.17

gin here »

and Fig.18 for the two nucleon transfer have been performed using optical model parameters and deformation values which fit the experimental data on ^{18}O and ^{16}O elastic and inelastic scattering. As previously suggested by N.K. Glendenning and G. Wolschin [32] the coupling with the ^{18}O 2^+ state was found to modify significantly the angular distribution of the g-s to g-s transition. Neglecting this transition, the calculated grazing peak was shifted by 4 degrees to backward angles producing a poorer agreement with the experimental data. The two step route via the ^{18}O 2^+ state produces an enhancement of the forward angle cross-section, moving the grazing peak in this direction. The importance of the ^{18}O 2^+ coupling was expected in the $^{76}Ge(^{16}O, ^{18}O)^{74}Ge$ two neutron pick-up reaction as the transitions corresponding to the ^{18}O excited in its 2^+ state are favored by a factor 3.5 compared to those where the ^{18}O is left in its ground-state.

In addition to its success in reproducing the marked shape difference of the differential cross-section observed experimentally between different final states, it has been shown that the relative intensities are better reproduced with CCBA calculations than with DWBA calculations [33,34,35]. Few examples are given in table II with the corresponding references.

D - The absolute magnitude problem

A common problem of two nucleon transfer reactions is that theoretical analysis generally underestimates the absolute cross-sections by one to two orders of magnitude. In dealing with comparison of absolute cross-sections obtained for different reactions it is necessary to also compare the method used for the calculations. In particular, the no recoil approximation overestimates the cross-sections by a factor 4 compared to the exact finite range calculation [36].

The work of T. Takemasa [37] shows that the cluster approximation with $\tilde{\ell} = 0$ relative motion is a good approximation to the microscopic form factor for targets as heavy as Ni. In contrast for lighter targets like ^{12}C the coherent summation of $\tilde{\ell} = 0,1,2$ and 3 terms increases the magnitude of the cross-section calculated by using only the $\tilde{\ell} = 0$ term by about 30%. Therefore the cluster approximation should be used with caution on light target nuclei.

The difficulty of too small theoretical cross-sections has been solved by the Texas group [38] for several two neutron and two proton transfer reactions. They show that the simultaneous transfer cross-section can be increased by a factor 2 by using extended shell model wave functions and taking into account of the residual interaction between the two nucleons. In addition, sequential transfer like $(^{18}O, ^{17}O)(^{17}O, ^{16}O)$ has cross-sections as large as simultaneous transfer. As the simultaneous and sequential transfer cross-sections add coherently, they have been able to reproduce the experimental cross-sections of a few reactions [38]. It still remains to understand the case of two proton transfer reactions where factors as large as 100 have been obtained.

IV. THE FOUR NUCLEON TRANSFER REACTIONS

The most promising aspect of the study of multinucleon transfer reactions is to get informations on four nucleons correlations in nuclei. This section will be divided into three parts dealing with :

a) some of the successes obtained with the $(^6Li,d)$ reaction,

b) our present knowledge of the $(^{16}O, ^{12}C)$ reaction mechanism,

c) the correspondance between the α and two nucleon transfer reactions.

A - Investigation of α clustering via the $(^6Li,d)$ reaction

In the 1p- and 2s-1d shell nuclei, the $(^6Li,d)$ reactions have been extensively studied [39]. The cluster property of the ^6Li projectile strongly supports the hypothesis that these reactions proceed via the transfer of an α particle. With the cluster description the cross-section of the A(a,b)B reaction can be written :

gin here »

$$\frac{d\sigma}{d\Omega} \sim \left| \sum_{\substack{NL \\ N'L'}} A_{NL}^{ba} A_{N'L'}^{BA} B_{NL\,N'L'}(\theta) \right|^2 . \qquad (1)$$

In this formalism, the DWBA transition amplitude in obtained by multiplying the dynamical factor B( ) with the structure amplitudes A_{NL} and $A_{N'L'}$ and summing over all possible principal and orbital quantum numbers NL, N'L' describing the center of mass motion of the four nucleons in their initial and final states. These quantum numbers are restricted to satisfy the following harmonic oscillator energy conservation relation :

$$2N + L + 2n + \ell = \sum_{i=1}^{4} (2n_i + \ell_i) \qquad (2)$$

where n_i, ℓ_i are the shell model quantum numbers of the individual transferred nucleons and n.ℓ the quantum numbers describing the relative motion of the transferred particles. With the two assumptions of a 0s relative motion (n = 0, ℓ = 0) between the transferred particles and a single N value for the description of the center of mass motion, the cross-section can be factorized as follows :

$$\frac{d\sigma}{d\Omega}(\theta) = S_{ab}^{\alpha} S_{BA}^{\alpha} \left(\frac{d\sigma}{d\Omega}(\theta)\right)_{DWBA} . \qquad (3)$$

The S^{α} are spectroscopic factors, which can be derived by comparing the data to exact finite range DWBA calculations. As shown in table III very good agreements have been obtained between the relative spectroscopic factors of the (^{6}Li,d) reaction and those predicted by SU3 calculations for the members of the ^{28}Si ground-state band [40]. Similar agreements have been found for levels of the ^{24,25,26}Mg residual nuclei populated by the ^{20,21,22}Ne(^{6}Li,d) reaction [41].

Exact finite range DWBA calculations have also been applied to determine α spectroscopic strengths for nuclei from ^{20}Ne to ^{66}Zn [42] (Fig.19).

For the light nuclei, these spectroscopic strengths are in good agreement with SU(3) theory. The strong increase around A ∿ 40 and A ∿ 66 may reflect the mixing of configurations belonging to different major shells. Indeed for ^{40}Ca nucleus the spectroscopic strength has been derived assuming a $(2s\text{-}1d)^4$ configuration for the nucleons transferred, so that the number of nodes of the radial wave function is N' = 4 (eq.2). In fact, particle-hole admixtures have been well established in the description of ^{40}Ca ground-state wave function. Therefore one can expect contributions of $((fp)^2\text{-}(ds)^2)$ and $(fp)^4$ configurations in the description of the four particles transferred. Such configurations will require respectively N = 5 and N = 6 nodes in the description of cluster radial wave function. So that the factorization into a spectroscopic factor and a DWBA cross-section is not anymore valid. One has to perform the coherent summation on N' in eq.(1) to derive the theoretical cross-section. As the DWBA cross-section increases with increasing number of nodes, the neglect of such contributions can lead to too small theoretical cross-section and therefore too large spectroscopic strengths. It would be interesting to calculate spectroscopic amplitudes of α transfer from wave-functions which include core excitation [43] to know if the corresponding DWBA cross-sections can explain the enhancement of the experimental cross-section around A ∿ 40.

The study of the (^{6}Li,d) reaction has not been extended to targets heavier than 1f-2p shell targets as an attempt performed on ^{90}Zr has shown that the cross-sections are weak (few microbarns) and swamped by large yields coming from light contaminants. The use of heavier projectiles to investigate four nucleon correlations on heavier target nuclei has been prompted by the (^{16}O, ^{12}C) data taken at Saclay on (2p-1f) shell targets [44,45]. The corresponding spectra clearly displayed a strong selectivity to states lying in an excitation energy region where the number of states is known to be quite high. Currently, we are investigating

gin here »» the reaction mechanism of the (^{16}O, ^{12}C) reaction to determine if it can be used to study α clustering property of these heavier nuclei as an alternative to the (^{6}Li,d) reaction.

B - Reaction mechanism of the (^{16}O, ^{12}C) four nucleon transfer

The question whether the four nucleons transferred in the (^{16}O, ^{12}C) reaction behave like an α particle has been the purpose of many discussions. Shell model calculations performed by D. Kurath and I. Towner [46] show that at the nuclear surface the contribution of 0s relative motion should dominate while all the other components (1p, 2s, 1d, 2p, 3s) of relative motion should have small cross-sections.

To check this hypothesis, experiments have been carried out to compare the (^{16}O, ^{12}C) reaction with the (^{6}Li,d) α transfer reaction. The experimental difficulty is to get energy spectra with an energy resolution similar to that obtained in the (^{6}Li,d) data. This is now possible with magnetic spectrometer having large solid angle and allowing for kinematic corrections. Fig.20 shows an energy spectrum of the $^{58}Ni(^{16}O, ^{12}C)^{62}Zn$ reaction measured with 65 keV energy resolution by means of the Saclay QDDD [47]. Comparing to the (^{6}Li,d) reaction, the same levels are excited. The strongest transitions are the same : the g-s 0^+ state, the 0.96 MeV 2^+ state, the 3.22 MeV 3^- state as well as the levels lying at 3.88 MeV, 4.04 MeV and 4.56 MeV excitation energies. In contrast the 1.80 MeV 2^+ state, the 2.18 MeV 4^+ and 2.74 MeV 3^- levels are weakly populated by both reactions. The correspondance between the states populated by the (^{16}O, ^{12}C) and the (^{6}Li,d) reactions has also been pointed out for the ^{40}Ca [48], ^{24}Mg and ^{28}Si targets [49]. However, the measured angular distributions of the ^{16}O, induced transitions are generally not reproduced by cluster transfer EFR-DWBA calculations, with optical model parameters derived from the elastic scattering data. This problem is similar to that encountered in the (^{16}O, ^{14}C) two proton transfer and has not been as yet solved.

One can obtain DWBA fits to the observed angular distributions by arbitrarily readjusting the optical model parameters. Such DWBA fits yield relative α spectroscopic factors which agree with the values obtained in a study of the (^{6}Li,d) reaction (Table III).

Comparisons of alpha widths derived from α decay to those obtained in a DWBA analysis of the (^{16}O, ^{12}C) reaction have been performed [50]. Their good agreement again suggests that the four nucleons are transferred in a 0s relative motion in the (^{16}O, ^{12}C) reaction (Table IV).

Nevetheless, there are also few experimental observations of population of unnatural parity states (Fig.21) by the (^{16}O, ^{12}C) reaction [49]. Such transitions are forbidden in a pure direct α transfer on a 0^+ target. The excitation of such unnatural parity states with significant cross-section implices that either the four nucleons are transferred in a relative motion different from 0s (op for instance) or multistep contributions via the inelastic excitation of the target or residual nuclei.

The failure of the DWBA formalism in reproducing angular correlation measurements of the $^{16}O(^{16}O, ^{12}C)^{20}Ne^{*} \rightarrow \alpha + ^{16}O$ sequential process also suggests that the (^{16}O, ^{12}C) reaction is not proceeding via a pure direct α transfer [51]. The Orsay group has shown that DWBA calculations which reproduce the transfer angular distributions do not dit the angular correlation data. Such experiment is a very powerful test of the reaction mechanism as it corresponds to the measurement of magnetic substate population.

C - On the correspondance between two and four nucleon transfer reactions

Spectroscopic amplitude calculations of α transfer have suggested a strong correlation between these α transfer and the two nucleon transfer reactions [46]. The spectroscopic strengths of the (d,^{6}Li) reaction measured on tin [52] and rare earth targets [53] well display such a correspondance between the (t,p) and (d,^{6}Li) data.

gin here ▸▸

Recent measurements of the (^{6}Li,d) reaction on ^{54,56,58}Fe isotopes [54] have confirmed the observation of a similarity between the (^{6}Li,d) and (t,p) spectra leading to the same residual nuclei. The only exceptions are the 0^+ states lying near 3.5 MeV excitation energy which are weakly excited by (t,p) and rather strongly by the (^{6}Li,d) reactions. These levels have been previously observed in the (^{3}He,n) reaction and interpreted as the proton-pairing vibrational states of Z = 28 closed shell. Their excitation of such states by the (^{6}Li,d) reaction has been used to investigate the proton pairing vibrational state of ^{62}Ni which was unknown. They identified it to the 0^+ state lying at 3.52 MeV excitation energy.

The energy spectra obtained for the (^{16}O, ^{14}C) and (^{16}O, ^{12}C) reactions leading to the same residual nucleus also display similar features. The differences in excitation energy region favored by the two reactions just reflect differences on ground-state Q values. In the excitation energy region where the two reactions can be compared they exhibit a similar selectivity [44,45].

V. CONCLUSION

The discussion on the ^{16}O + ^{28}Si elastic scattering has shown that neither the validity nor the parameters of an optical model describing the interaction of two heavy ions are determined.

The semi-classical theory concluding complex trajectories is a powerful tool to investigate the physical origin of the observed angular distributions.

Both elastic and target inelastic angular distributions are generally well described in terms of coupled channel formalism. In contrast, the ^{18}O 2^+ projectile inelastic angular distribution is still a problem.

The study of two nucleon transfer reactions induced by heavy ions has pointed out important contributions of two step process where the transfer is proceeding via target and residual nucleus inelastic excitation. At incident energies not too high above the Coulomb barrier, such process produces clear shape changes between different final state angular distributions. At higher incident energy, the angular distributions are forward peaked and display oscillations for both mechanisms. Nevertheless the failure of DWBA theory in reproducing the cross-section of different final states with the same normalization factor is generally removed by using CCBA formalism.

Normalization factors close to 1 have been obtained between theoretical and experimental cross-sections, by taking into account of sequential transfer in addition to simultaneous transfer.

Concerning the (^{16}O, ^{12}C) reaction, the reaction mechanism has not been so much studied. The existing data suggest that the four nucleons are well transferred into a 0s relative motion. Further investigations are required to understand why the DWBA failed to reproduce angular distributions and experimental cross-sections.

ACKNOWLEDGMENT

I could like to thank Dr. K.S. Low for many fruitful discussions and collaborations. The semi-classical calculations have been performed in collaboration with Dr. R. Schaeffer. I would like to take this opportunity to thank him.

gin here »

REFERENCES

1) D.G. Kovar, Procs. Conf. on reactions between complex nuclei, Nashville (North-Holland) vol.2 (1974) 235.

2) A.J. Baltz, Symposium on macroscopic features on heavy ion collisions, Argonne Illinois, April 1976, vol.1, 65.

3) K.S. Low, European Conference on nuclear physics with heavy ions, Caen, 1976, 75.

4) R. Satchler, Symposium on macroscopic features on heav- ion collisions, Argonne, Illinois, April 1976, vol.1, 33.

5) D.M. Brink, European Conference on nuclear physics with heavy ions, Caen, 1976 47.

6) J.C. Cramer et al., Phys. Rev. C14 (1974) 2158.

7) P. Braun-Munziger et al., Phys. Rev. Lett. 38 (1977) 944.

8) R. Satchler, Nucl. Phys. A279 (1977) 493.

9) J. Knoll and R. Schaeffer, Ann. Phys. (N.Y.) 97 (1976) 307 ; Phys. Reports, to be published.

10) P. Charles et al., Phys. Lett. 62B (1976) 289 ; U.C. Voos et al., Nucl. Phys. A135 (1969) 207.

11) P.J. Moffa et al., Phys. Rev. C13 (1976) 147.

12) O. Hansen and J.D. Garrett, Proceeding on European Conference on nuclear physics with heavy ions, Caen, 1976, 1.

13) R. Schaeffer and M.-C. Lemaire, Contribution to this Conference.

14) R.A. Malfiet et al., Phys. Lett. 44B (1973) 238.

15) W.F. Frahn, Heavy ion high spin states and nuclear structure, (IAEA, Vienna) vol.1 (1975) 157.

16) R. da Silveira, Phys. Lett. 45B (1973) 211.

17) P.D. Bond et al., Phys. Rev., to be published.

18) M. Cobern et al., Phys. Rev. C13 (1976) 674.

19) J. Carter et al., Nucl. Phys. A273 (1976) 523.

20) D.L. Hillis et al., Phys. Rev. Lett. 36 (1976) 304.

21) C.E. Thorn et al., Phys. Rev. Lett. 38 (1977) 384.

22) K.E. Rehm et al., Phys. Rev. C12 (1975) 1945.; F. Videbaek et al., Nucl. Phys. A256 (1967) 301.

23) Previous reviews of these data can be found in the following conference proceedings ; Reactions induced by heavy ions, ed. by R. Bock and W.R. Herring (North-Holland, Amsterdam 1970) ; Symposium on heavy in reactions and many particle excitations (Saclay, 1971) J. Phys. 32 (1971) C6 ; European conference on nuclear physics (Aix-en-Provence, 1972) J. Phys. 33 (1972) C5 ; ORNL Heavy ion summer study (Oak Ridge, 1972) ; Symposium on heavy ion transfer reactions (Argonne, March 1973) ; International conference on nuclear physics (Munich, 1973) ; Reaction between complex nuclei, ed. by R.L. Robinson, F.K. McGowan, J.B. Ball, J.M. Hamilton (North-Holland, Nashville 1974) 235.

24) M. Conjeaud et al., Nucl. Phys. A250 (1975) 182.; M.-C. Lemaire et al., Phys. Rev. C10 (1974) 1103.

25) Y. Eisen et al., Phys. Rev. C12 (1976) 699.

26) M. Bernas et al., Contribution to this conference.

27) R. Middleton and J. Pullen, Nucl. Phys. 51 (1964) 77.

gin here »

28) B. Rastegar., Nucl. Phys. A225 (1974) 80.

29) M.E. Cobern et al., Phys. Rev. C13 (1976) 1200.

30) P.D. Bond et al., Phys. Rev. to be published.

31) M.-C. Lemaire and K.S. Low, Phys. Rev. to be published.

32) N.K. Glendenning and G. Wolschin, Phys. Rev. Lett. 34 (1975) 1642.

33) M.C. Mermaz et al., Phys. Rev. C15 (1977) 307.

34) M. Conjeaud et al., Contribution the European Conference on nuclear physics with heavy ions, Caen, 1976, 35.

35) B. Sorensen, Phys. Lett. 33B (1974) 285.

36) B.F. Bayman, Phys. Rev. Lett. 32 (1974) 71.

37) T. Takemasa, Phys. Rev. C13 (1976) 2343 ; Phys. Lett. 55B (1975) 28.

38) D.H. Feng et al., Phys. Rev. C4 (1976) 1484 ; Nucl. Phys. A274 (1976) 262.

39) K. Bethge, Ann. Rev. Nucl. Science, 20 (1970) 255.

40) J.P. Draayer et al., Phys. Lett. 53B (1974) 250.

41) N. Anantaraman et al., Nucl. Phys. A279 (1977) 474.

42) N. Anantaraman et al., Phys. Rev. Lett. 35 (1975) 1131.

43) A. Zuker, Proceeding of the topical conference on the structure of $1f_{7/2}$ nuclei, Padova (1971).

44) H. Faraggi et al., Phys. Rev. C4 (1971) 1375 ; Ann. Phys. (N.Y.) 66 (1971) 1375 ; Phys. Rev. Lett. 24 (1970) 1188.

45) M.-C. Lemaire, Phys. Reports 7C (1973) n°6.

46) D. Kurath and I. Towner, Nucl. Phys. 22 (1971) 1.

47) B. Berthier et al., Contribution to the European Conference on nuclear physics with heavy ions, Caen (1976) 53.
Rapport CEA (1976) 37.

48) J.R. Erskine et al., Phys. Lett. 47B (1973) 335.

49) J.C. Peng et al., Nucl. Phys. A264 (1976) 312.

50) R.M. DeVries et al., Phys. Rev. Lett. 35 (1975) 835 ; W.G. Davies et al., Nucl. Phys. A269 (1976) 477.

51) P. Roussel et al., Contribution to the European Conference on nuclear physics with heavy ions, Caen (1976) 38 ; F. Pougheon, Contribution to the Bormio Winter School, January (1977) ; B. Fabro, Thesis, Orsay 1977.

52) F. Becchetti et al., Phys. Rev. Lett. 35 (1975) 268.

53) F.L. Milder et al., to be published.

54) N. Stein et al., Phys. Rev. Lett. 38 (1977) 587.

:gin here »

FIGURE CAPTIONS

Fig.1 Angular distributions of the $^{16}O + ^{28}Si$ elastic scattering [Ref.6].

Fig.2 Experimental evidence of backward angle oscillations in the $^{16}O + ^{28}Si$ elastic scattering angular distribution [Ref.7].

Fig.3 Comparaison of the quantal and semi-classical calculations of $^{16}O + ^{28}Si$ elastic scattering angular distributions.

Fig.4 Trajectories included in the semi-classical calculations [Ref.9].

Fig.5 Contributions of the differents trajectories to the semi -classical cross-section at 33 and 50 MeV incident energies.

Fig.6 Contribution of the differents trajectories to the $^{16}O + ^{28}Si$ elastic cross-section at 215.2 MeV incident energy.

Fig.7 Invetigation of the respective role played by the real and imaginary part of the optical potential in the description of the elastic scattering angular distribution [Ref.13].

Fig.8 The $^{74}Ge(^{18}O, ^{18}O)^{74}Ge$ elastic and inelastic angular distributions [Ref.30].

Fig.9 The $^{76}Ge(^{16}O, ^{16}O)^{76}Ge$ elastic and inelastic angular distributions [Ref.30].

Fig.10 Elastic and inelastic angular distributions.

Fig.11 The $^{18}O^{*}$ 2^{+} projectile inelastic angular distribution [Ref.30].

Fig.12 Energy spectra of the $^{42,48}Ca(^{16}O, ^{14}C)^{44,50}Ti$ reactions [Ref.25].

Fig.13 Energy spectrum of the $^{26}Mg(^{18}O, ^{16}O)^{28}Mg$ reaction [Ref.26].

Fig.14 Angular distributions of the $^{48}Ca(^{16}O, ^{14}C)^{50}Ti$ reaction [Ref.25].

Fig.15 Angular distributions of the ^{28}Mg ground-state and first 2^{+} state populated by the $^{26}Mg(^{18}O, ^{16}O)^{28}Mg$ reaction [Ref.26].

Fig.16 Angular distributions of the $^{72,74,76}Ge(^{16}O, ^{14}C)^{74,76,78}Se$ transitions leading to the ground-state, first 2^{+} and 3^{-} excited states [Ref.29].

Fig.17 Angular distributions of the $^{76}Ge(^{16}O, ^{18}O)^{74}Ge$ reaction [Ref.31].

Fig.18 Angular distributions of the $^{74}Ge(^{18}O, ^{16}O)^{76}Ge$ reaction [Ref.31].

Fig.19 Alpha spectroscopic strengths determined from the $(^{6}Li,d)$ reaction on target nuclei ranging from ^{16}O to ^{64}Ni.

Fig.20 High resolution energy spectrum of the $^{58}Ni(^{16}O, ^{12}C)^{62}Zn$ reaction measured with the Saclay QDDD [Ref.47].

Fig.21 Population of unnatural parity states in the $(^{16}O, ^{12}C)$ reaction [Ref.49].

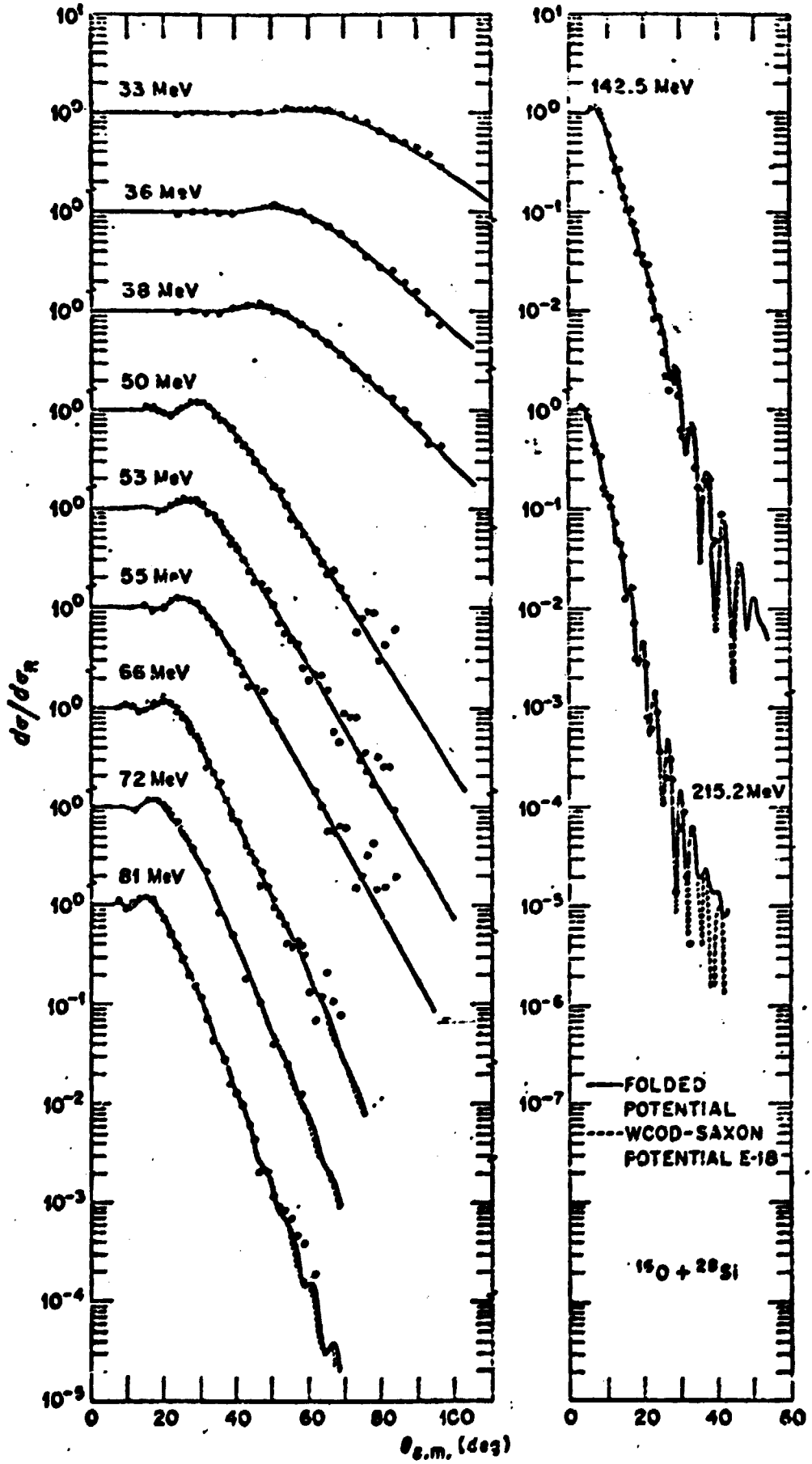
33 MeV
36 MeV
38 MeV
50 MeV
53 MeV
55 MeV
66 MeV
72 MeV
81 MeV
142.5 MeV
215.2MeV
dσ/dσR
θc.m. (deg)
FOLDED POTENTIAL
WOOD-SAXON POTENTIAL E-18
16O + 28Si

Fig.1

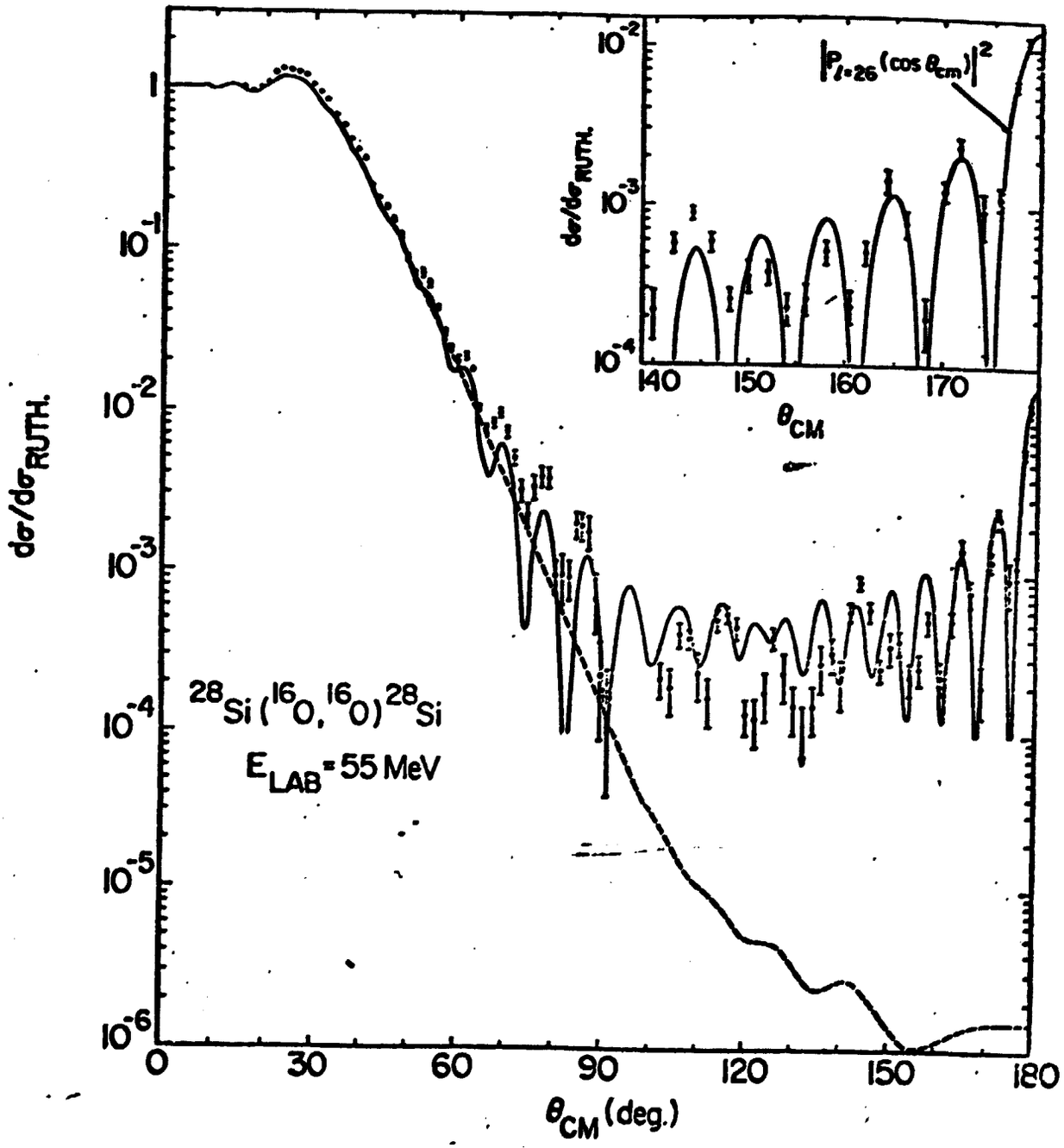
$^{28}Si(^{16}O,^{16}O)^{28}Si$
E_{LAB} = 55 MeV
$d\sigma/d\sigma_{RUTH.}$
θ_{CM} (deg.)
$|P_{l=26}(\cos\theta_{cm})|^2$
θ_{CM}

Fig.2

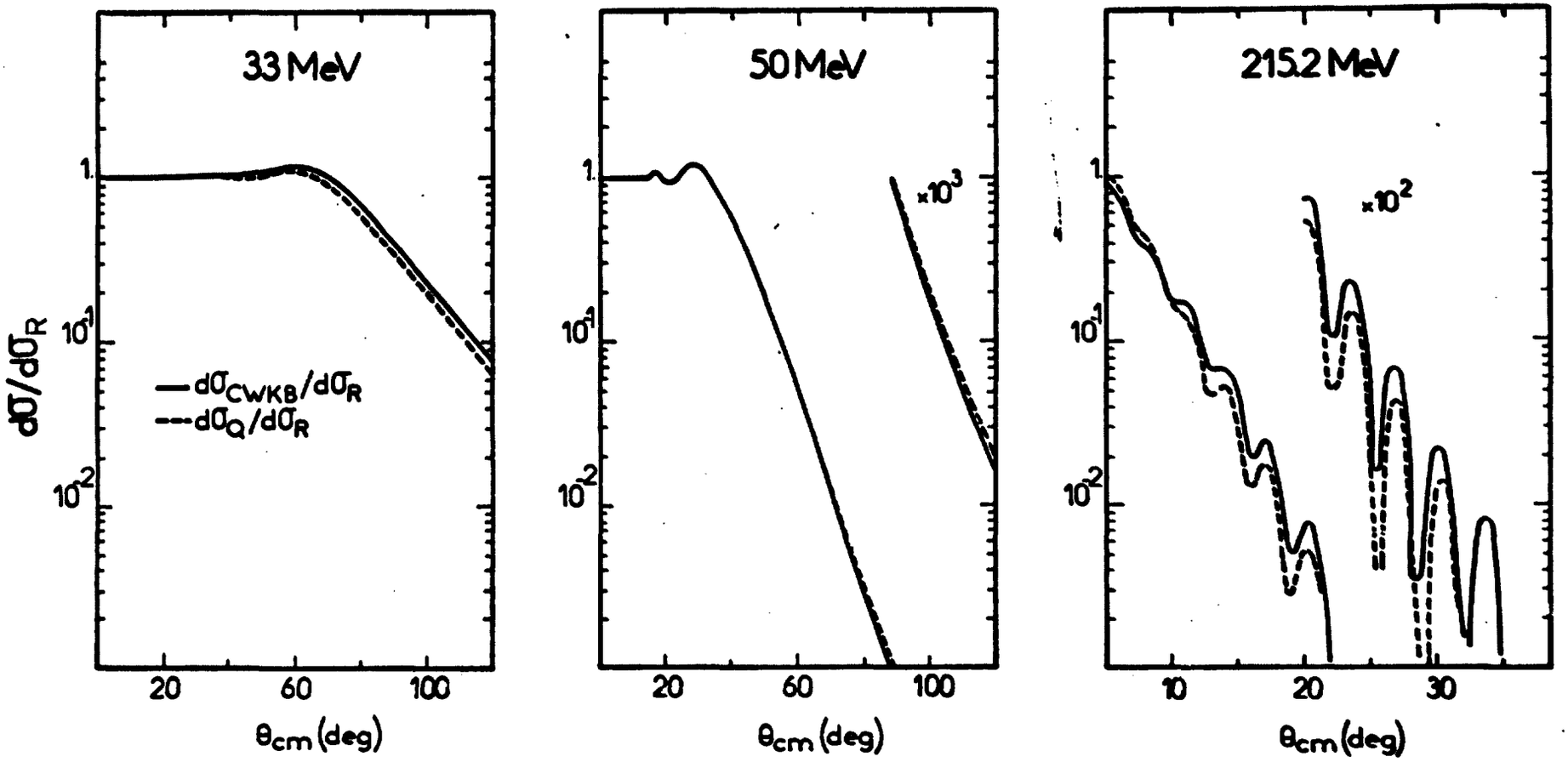
33 MeV
50 MeV
215.2 MeV
dσ/dσR
dσCWKB/dσR
dσQ/dσR
×10³
×10²
θcm (deg)
θcm (deg)
θcm (deg)

Fig.3

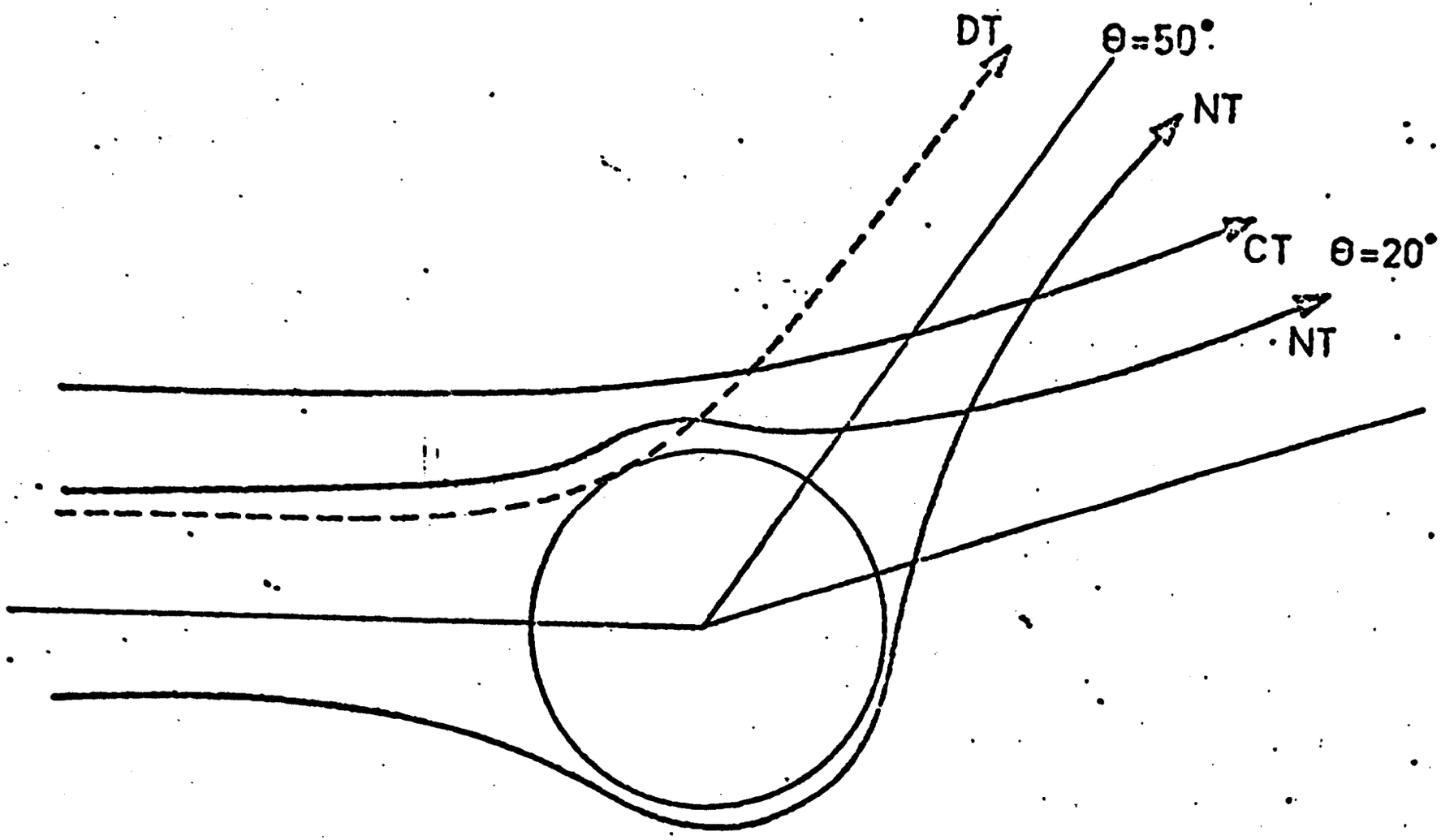

Fig.4

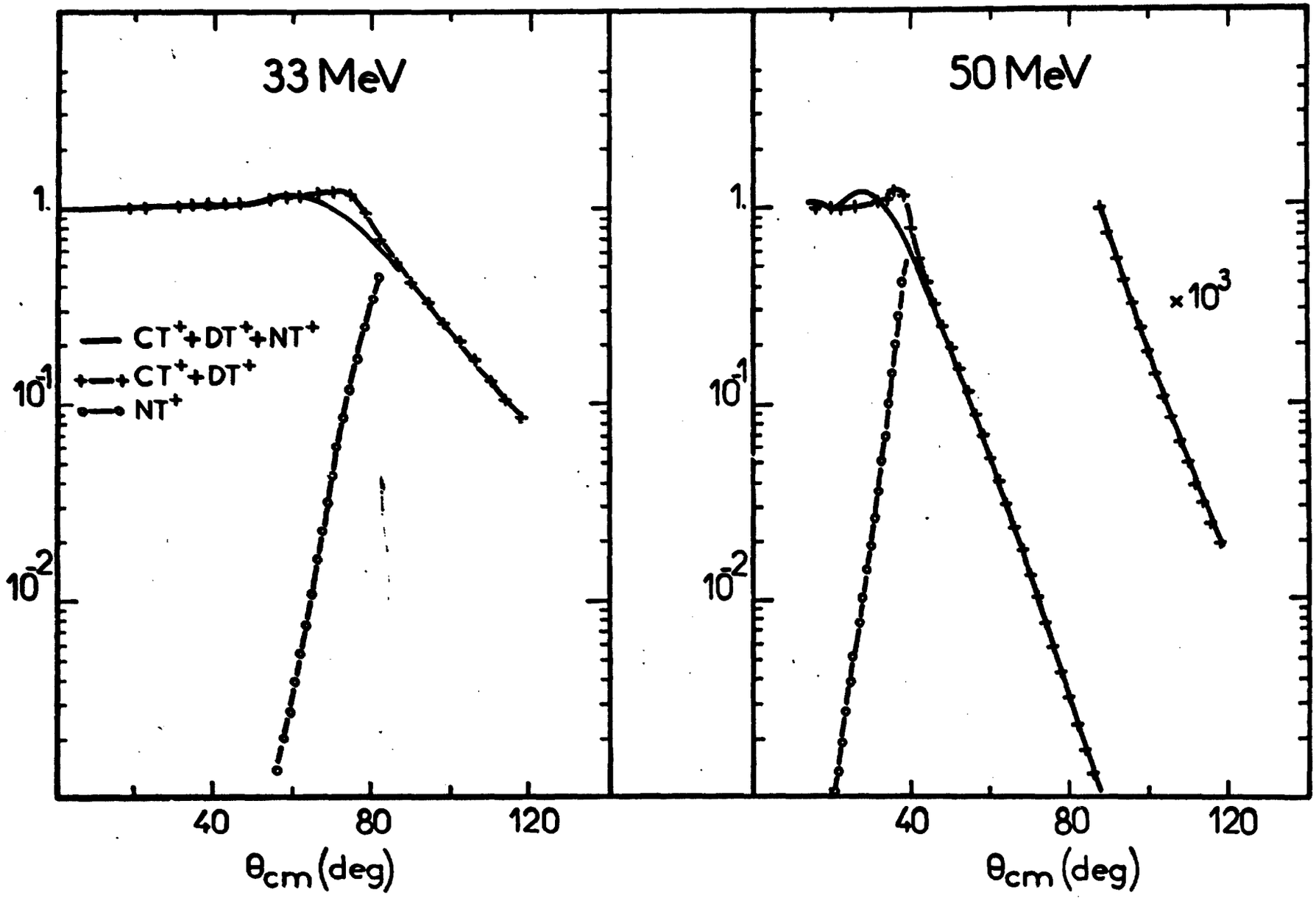
33 MeV
50 MeV
1.
10^{-1}
10^{-2}
$CT^+ + DT^+ + NT^+$
$CT^+ + DT^+$
NT^+
$\times 10^3$
40
80
120
θ_{cm} (deg)

Fig.5

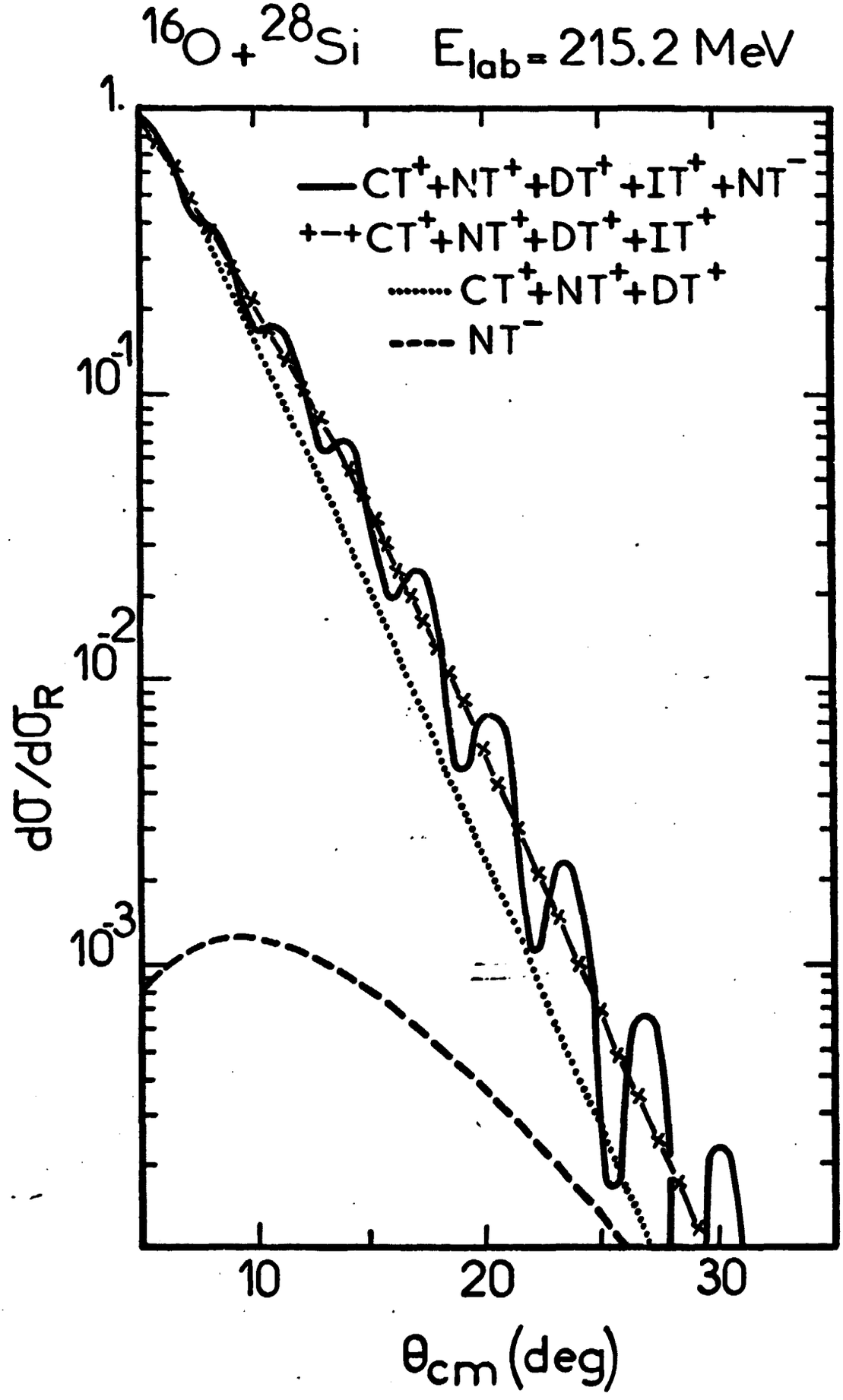
$^{16}O + ^{28}Si$ $E_{lab} = 215.2$ MeV
1.
10^{-1}
10^{-2}
10^{-3}
$d\sigma/d\sigma_R$
$CT^+ + NT^+ + DT^+ + IT^+ + NT^-$
$CT^+ + NT^+ + DT^+ + IT^+$
$CT^+ + NT^+ + DT^+$
NT^-
10
20
30
θ_{cm} (deg)

Fig.6

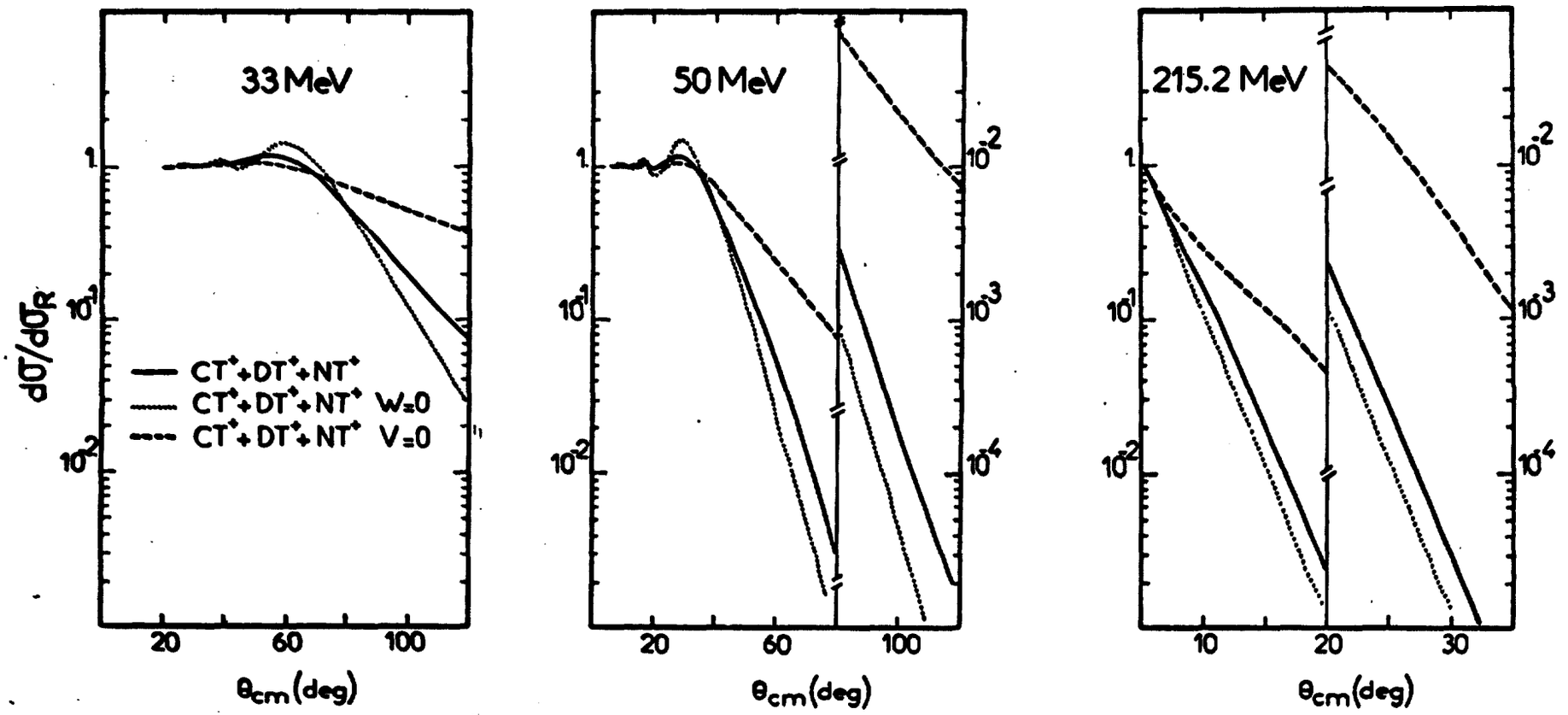
33 MeV
50 MeV
215.2 MeV
dσ/dσR
θcm(deg)
CT⁺+DT⁺+NT⁺
CT⁺+DT⁺+NT⁺ W=0
CT⁺+DT⁺+NT⁺ V=0

Fig. 7

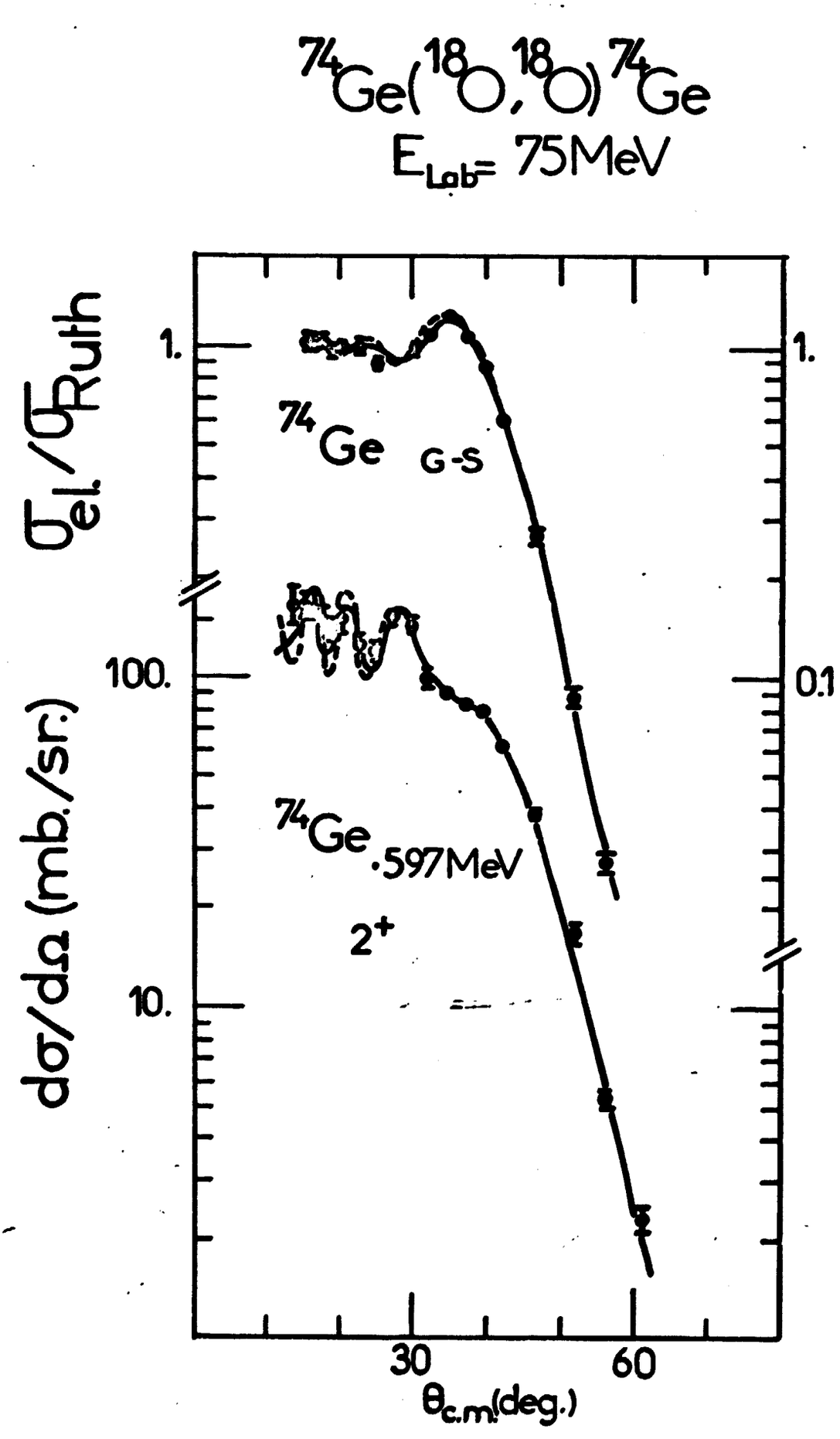
74Ge(18O,18O)74Ge
ELab= 75MeV
σel./σRuth
dσ/dΩ (mb./sr.)
1.
100.
10.
1.
0.1
74Ge G-S
74Ge .597MeV
2+
30
60
θc.m.(deg.)

Fig.8

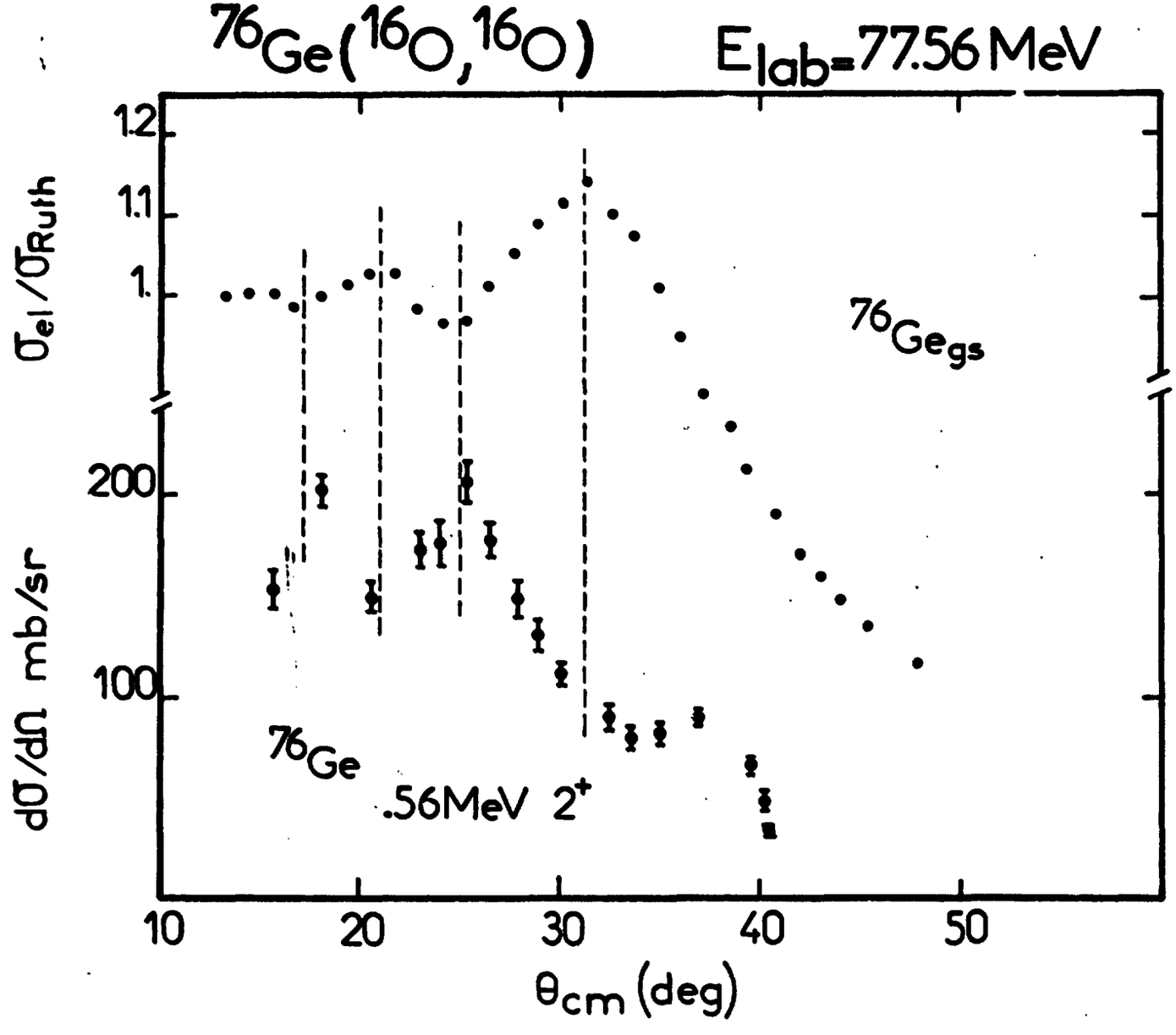
$^{76}Ge(^{16}O,^{16}O)$ E_{lab}=77.56 MeV
$\sigma_{el}/\sigma_{Ruth}$
$d\sigma/d\Omega$ mb/sr
1.2
1.1
1.
200
100
$^{76}Ge_{gs}$
^{76}Ge .56MeV 2^+
10
20
30
40
50
θ_{cm} (deg)

Fig.9

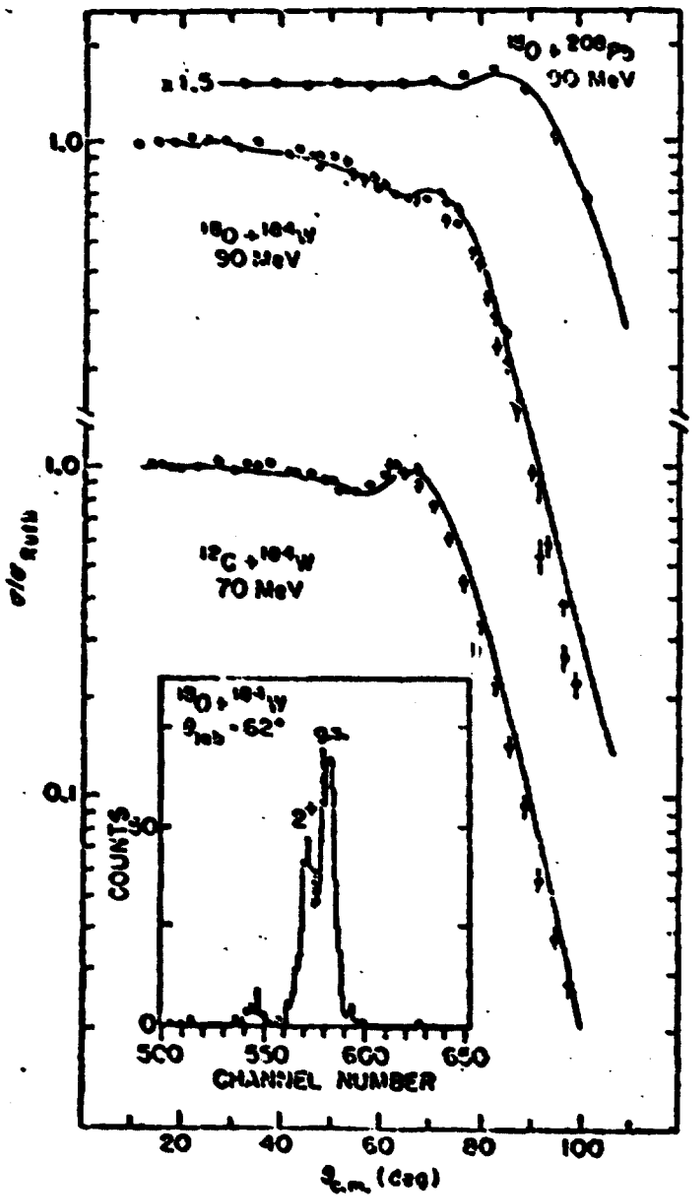
$^{18}O + ^{208}Pb$
90 MeV
a 1.5
1.0
$^{18}O + ^{184}W$
90 MeV
1.0
$^{12}C + ^{184}W$
70 MeV
0.1
σ/σ_{Ruth}
$^{18}O + ^{184}W$
$\theta_{lab} = 62°$
2+
COUNTS
30
0
500
550
600
650
CHANNEL NUMBER
20
40
60
80
100
$\theta_{c.m.}$ (deg)

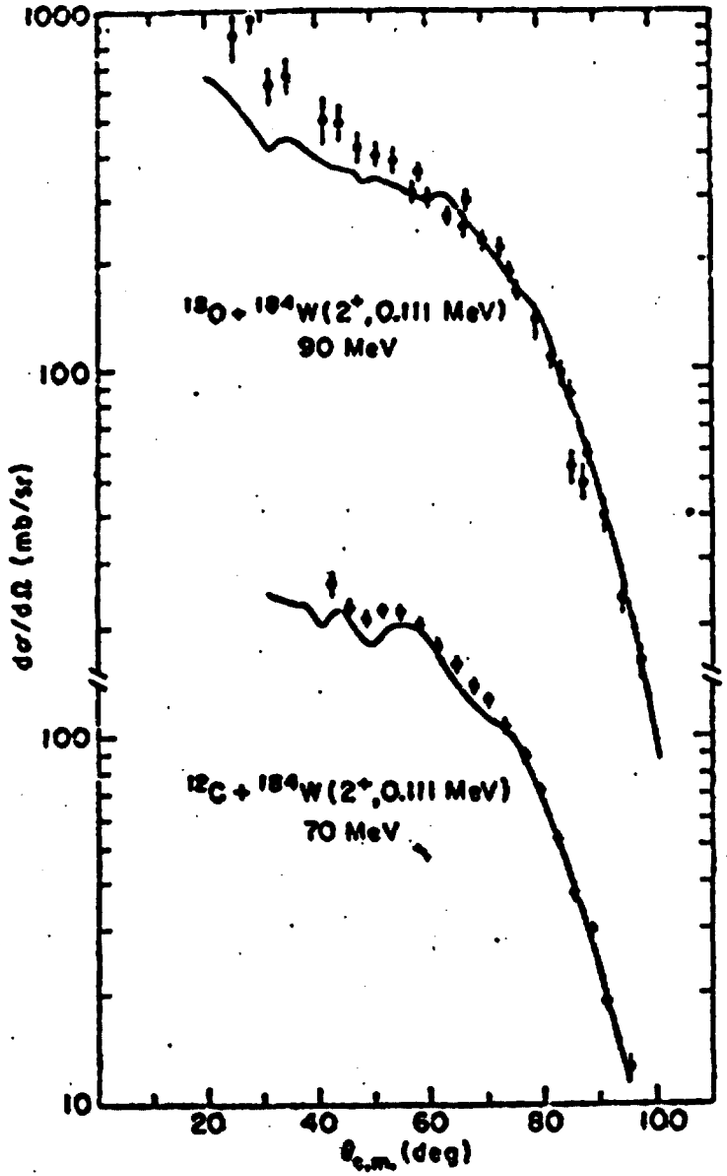
1000
100
$^{18}O + ^{184}W(2^+, 0.111$ MeV)
90 MeV
100
$^{12}C + ^{184}W(2^+, 0.111$ MeV)
70 MeV
10
$d\sigma/d\Omega$ (mb/sr)
20
40
60
80
100
$\theta_{c.m.}$ (deg)

Fig.10

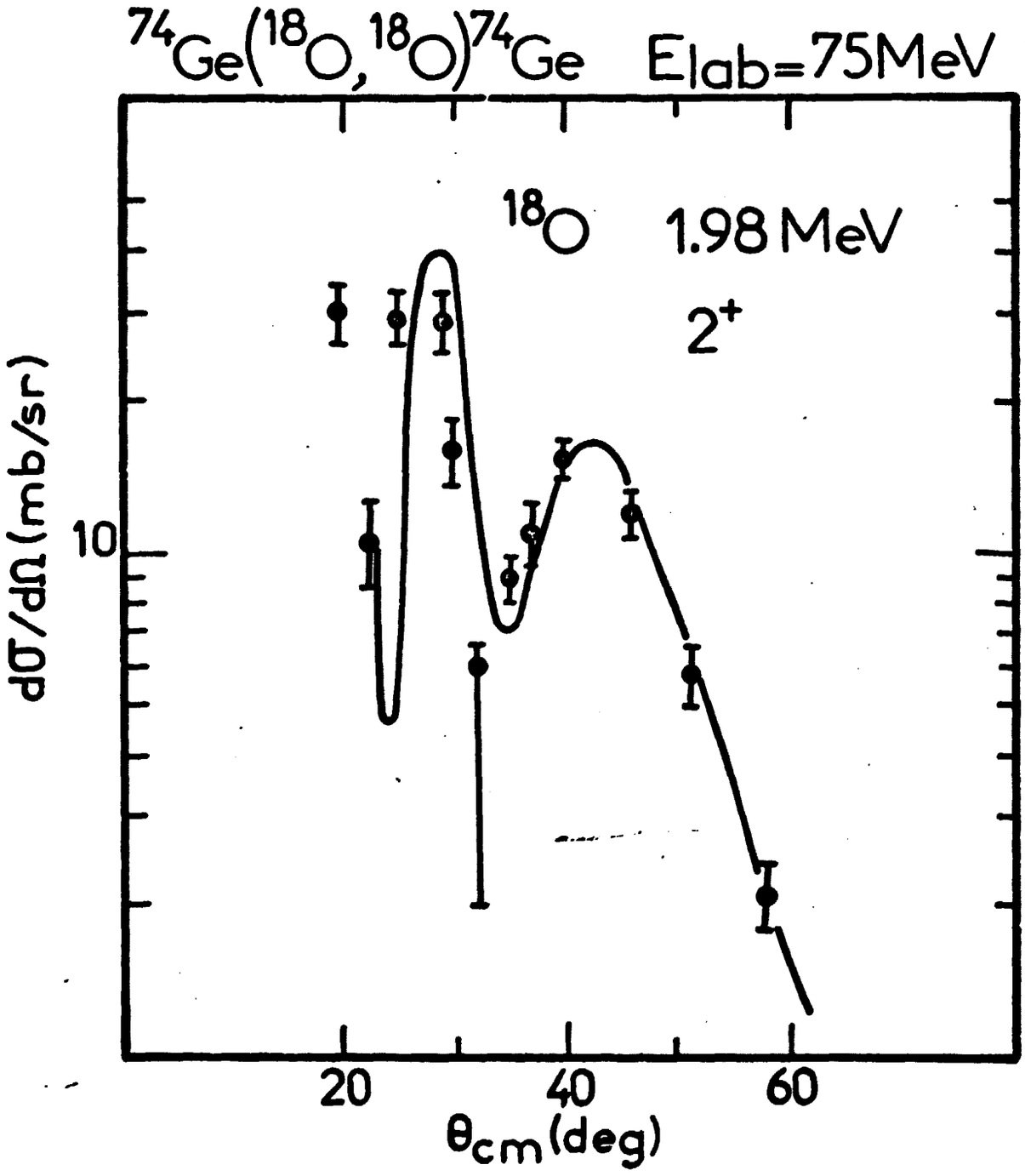
$^{74}Ge(^{18}O,^{18}O)^{74}Ge$ Elab=75MeV
^{18}O 1.98 MeV
2^+
$d\sigma/d\Omega$ (mb/sr)
10
20
40
60
θ_{cm} (deg)

Fig.11

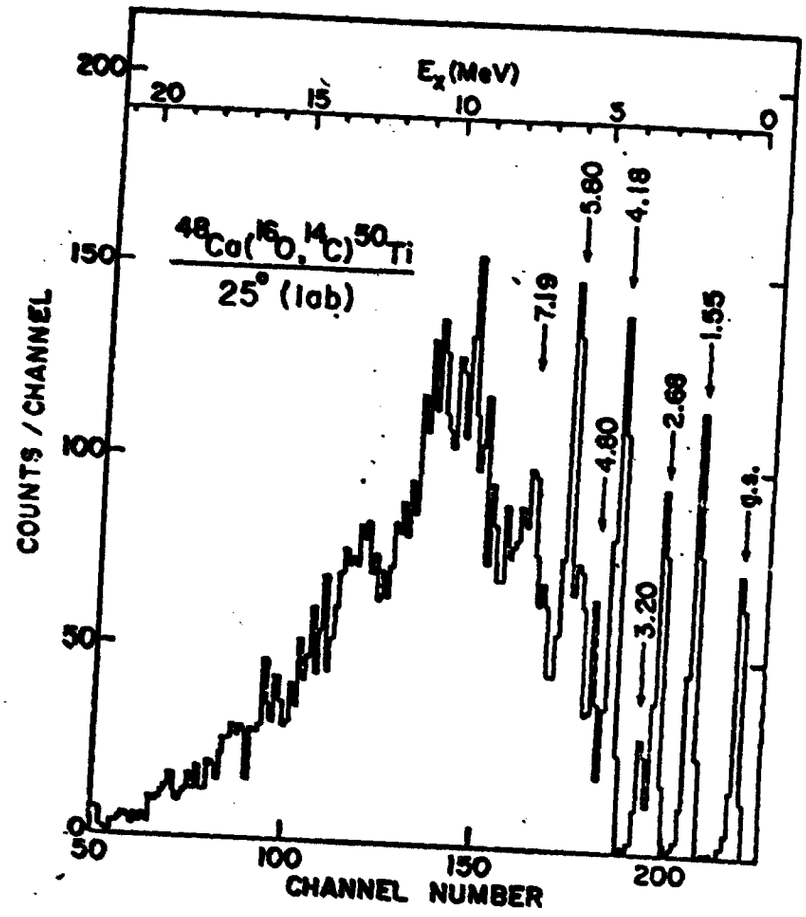
$^{48}Ca(^{16}O,^{14}C)^{50}Ti$
25° (lab)
E_x(MeV)
20
15
10
5
0
7.19
5.80
4.18
4.80
3.20
2.68
1.55
g.s.
COUNTS / CHANNEL
CHANNEL NUMBER
50
100
150
200

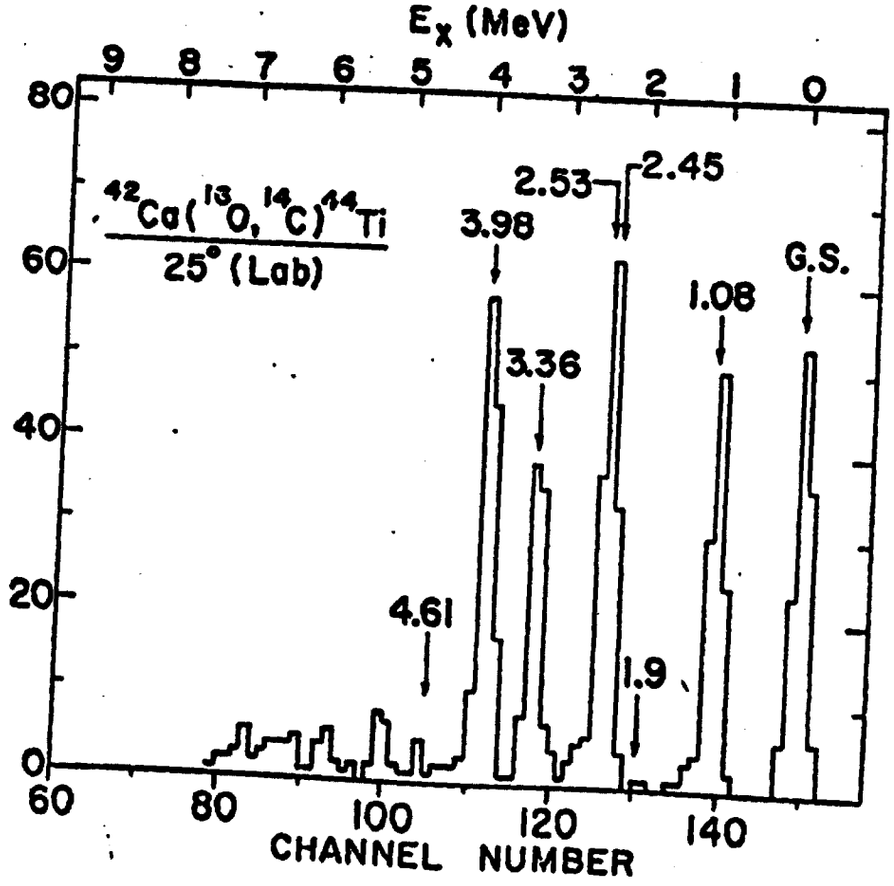
E_x (MeV)
9
8
7
6
5
4
3
2
1
0
$^{42}Ca(^{13}O,^{14}C)^{44}Ti$
25° (Lab)
4.61
3.98
3.36
2.53
2.45
1.9
1.08
G.S.
CHANNEL NUMBER
60
80
100
120
140

Fig. 12

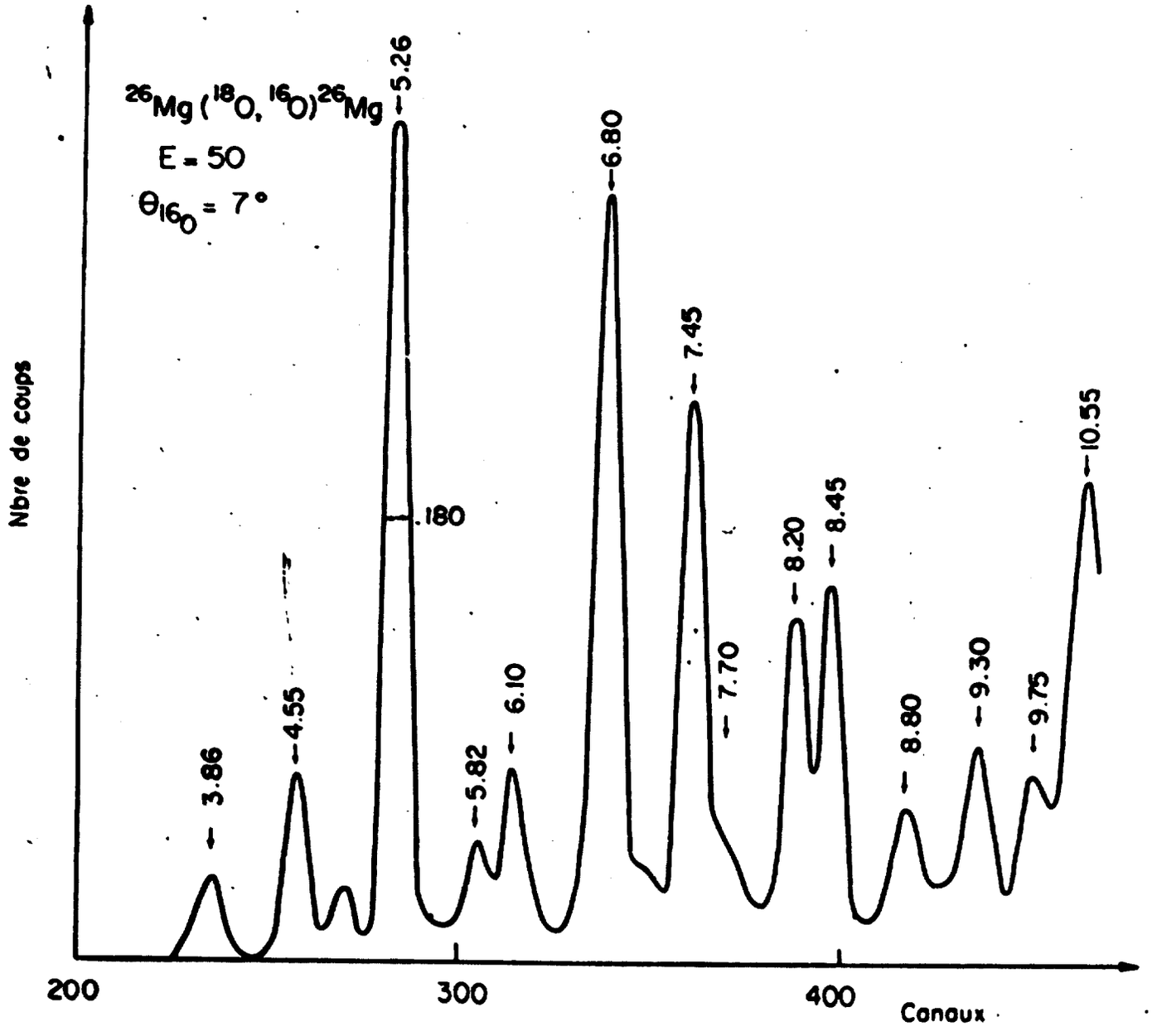
$^{26}Mg(^{18}O, ^{16}O)^{26}Mg$
E = 50
$\theta_{16_O} = 7°$
Nbre de coups
5.26
6.80
7.45
.180
10.55
8.20
8.45
4.55
6.10
7.70
3.86
5.82
8.80
9.30
9.75
200
300
400
Canaux

FIG. 13

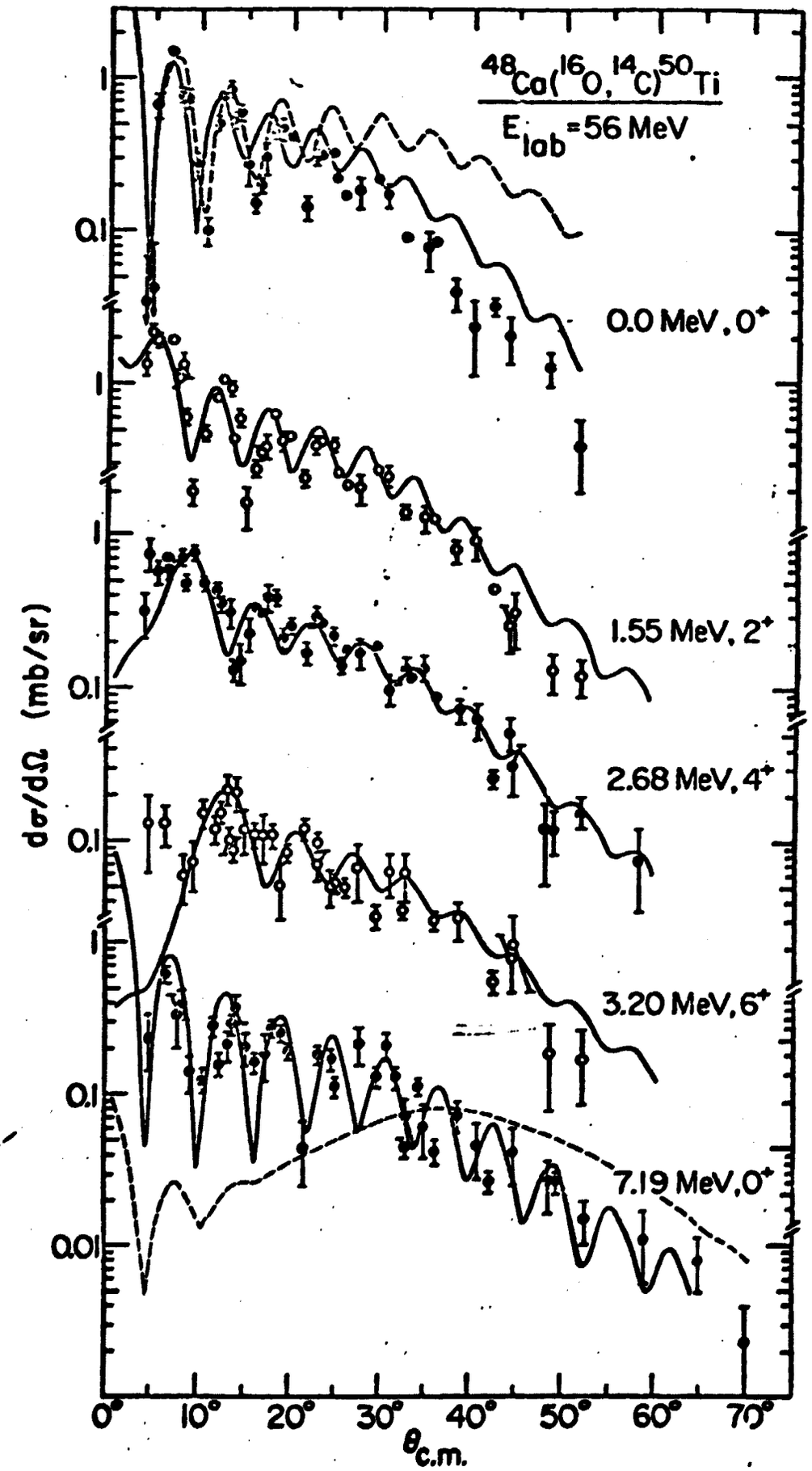
$^{48}Ca(^{16}O, ^{14}C)^{50}Ti$
E_{lab}=56 MeV
0.0 MeV, 0+
1.55 MeV, 2+
2.68 MeV, 4+
3.20 MeV, 6+
7.19 MeV, 0+
dσ/dΩ (mb/sr)
1
0.1
1
0.1
1
0.1
0.01
0°
10°
20°
30°
40°
50°
60°
70°
θc.m.

Fig. 14

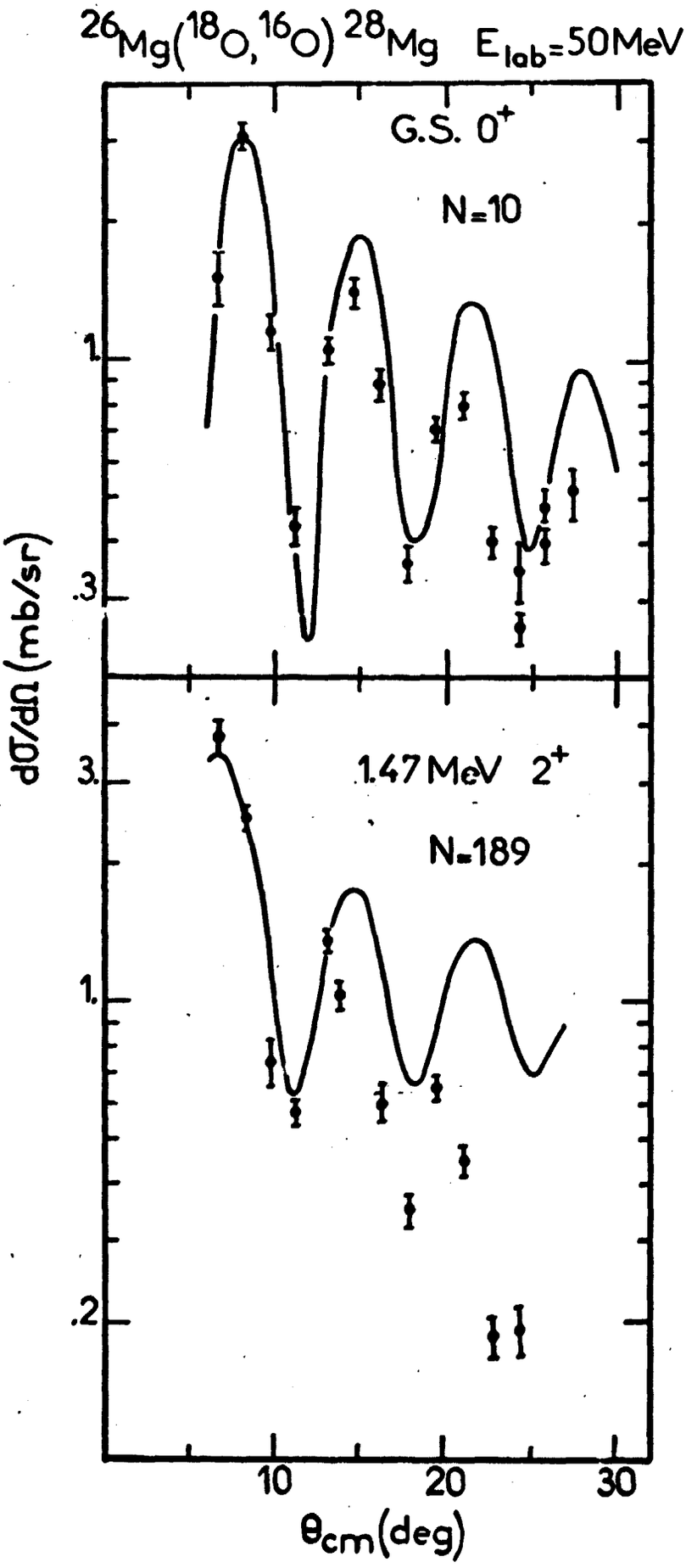
$^{26}Mg(^{18}O,^{16}O)^{28}Mg$ E_{lab}=50MeV
G.S. 0^+
N=10
1.
.3
1.47MeV 2^+
N=189
3.
1.
.2
10
20
30
θ_{cm}(deg)
dσ/dΩ (mb/sr)

Fig.15

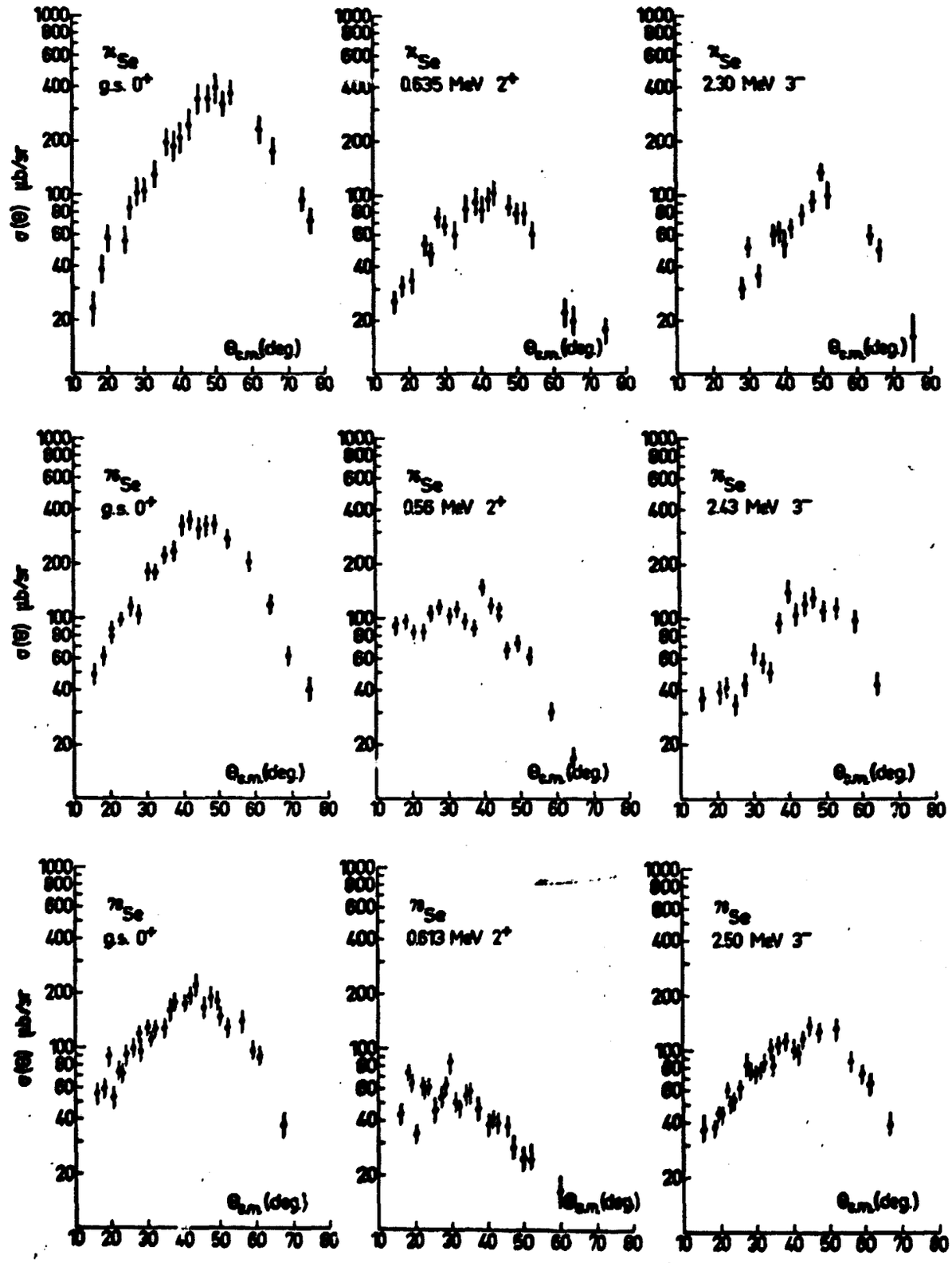
Ge (^{16}O, ^{14}C) Se $E_{^{16}O} = 56$ MeV
^{74}Se
g.s. 0$^+$
0.635 MeV 2$^+$
2.30 MeV 3$^-$
^{76}Se
g.s. 0$^+$
0.56 MeV 2$^+$
2.43 MeV 3$^-$
^{78}Se
g.s. 0$^+$
0.613 MeV 2$^+$
2.50 MeV 3$^-$
σ(θ) μb/sr
θ$_{c.m.}$(deg.)

Fig.16

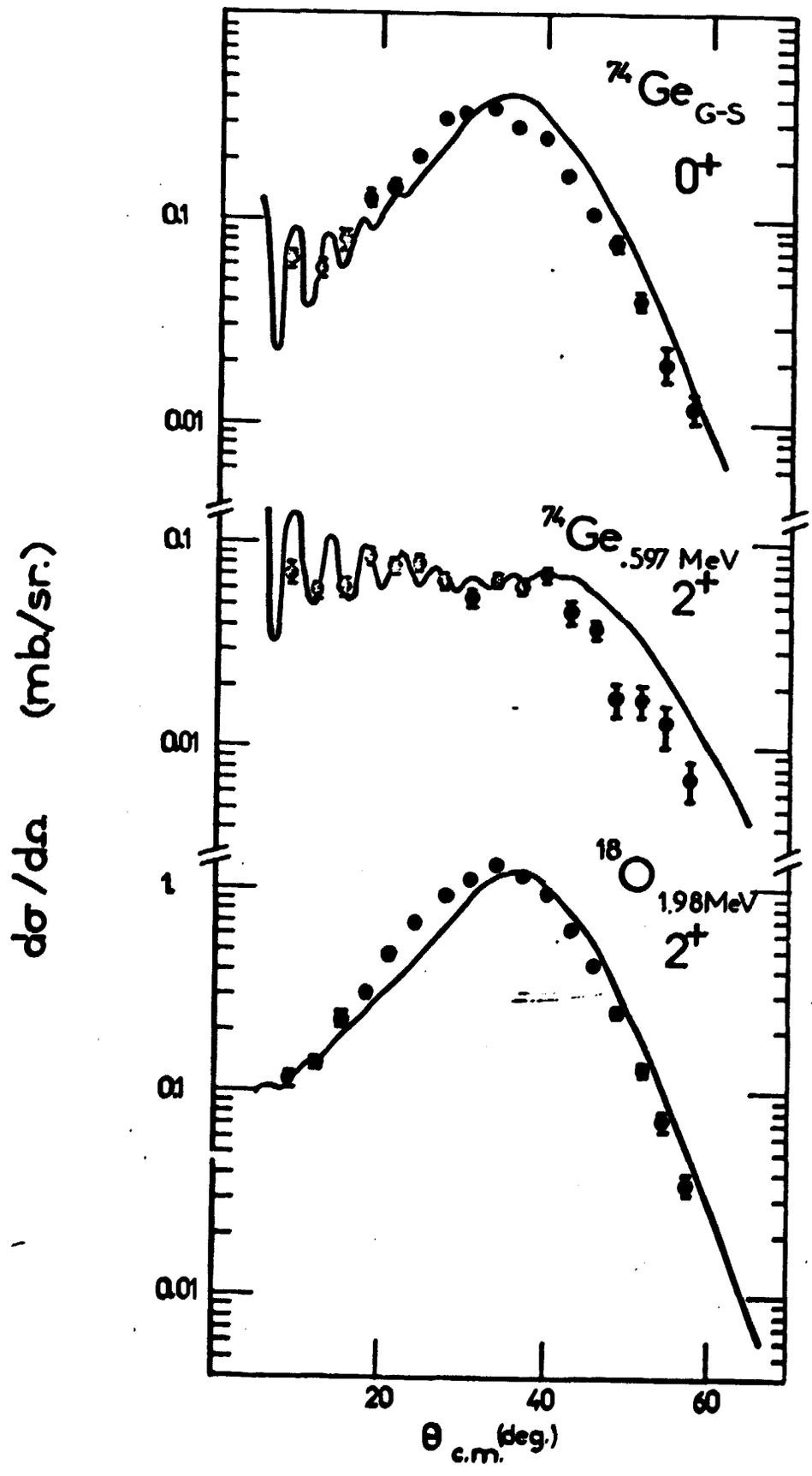
$^{76}Ge(^{16}O,^{18}O)^{74}Ge$
$^{74}Ge_{G-S}$
0^+
$^{74}Ge_{.597\ MeV}$
2^+
$^{18}O_{1.98MeV}$
2^+
0.1
0.01
0.1
0.01
1
0.1
0.01
20
40
60
$\theta_{c.m.}$ (deg.)
$d\sigma/d\Omega$ (mb/sr.)

Fig.17

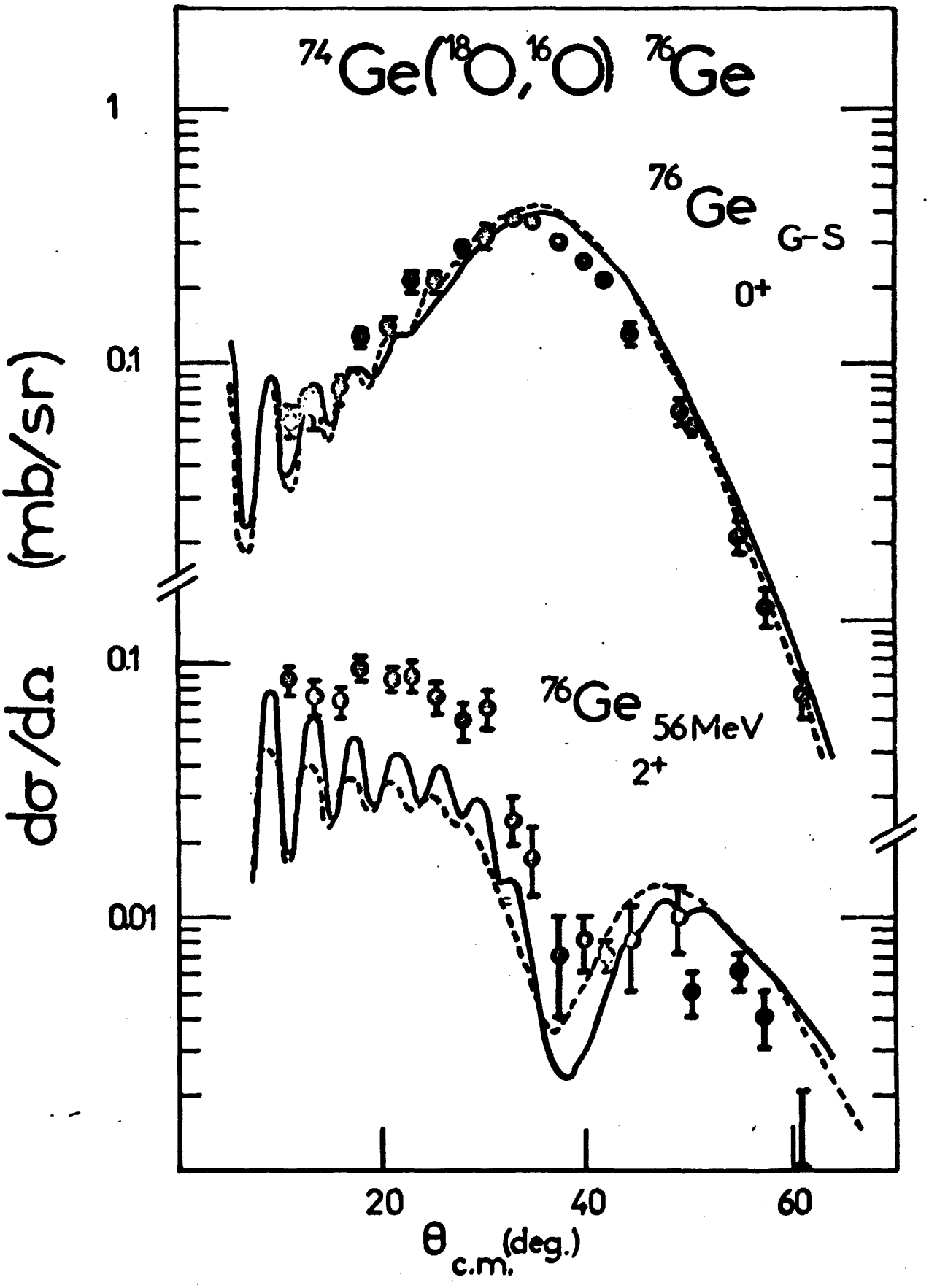
$^{74}Ge(^{18}O,^{16}O)\ ^{76}Ge$
^{76}Ge G-S
0^+
^{76}Ge 56MeV
2^+
1
0.1
0.1
0.01
$d\sigma/d\Omega$ (mb/sr)
20
40
60
$\theta_{c.m.}$(deg.)

Fig. 18

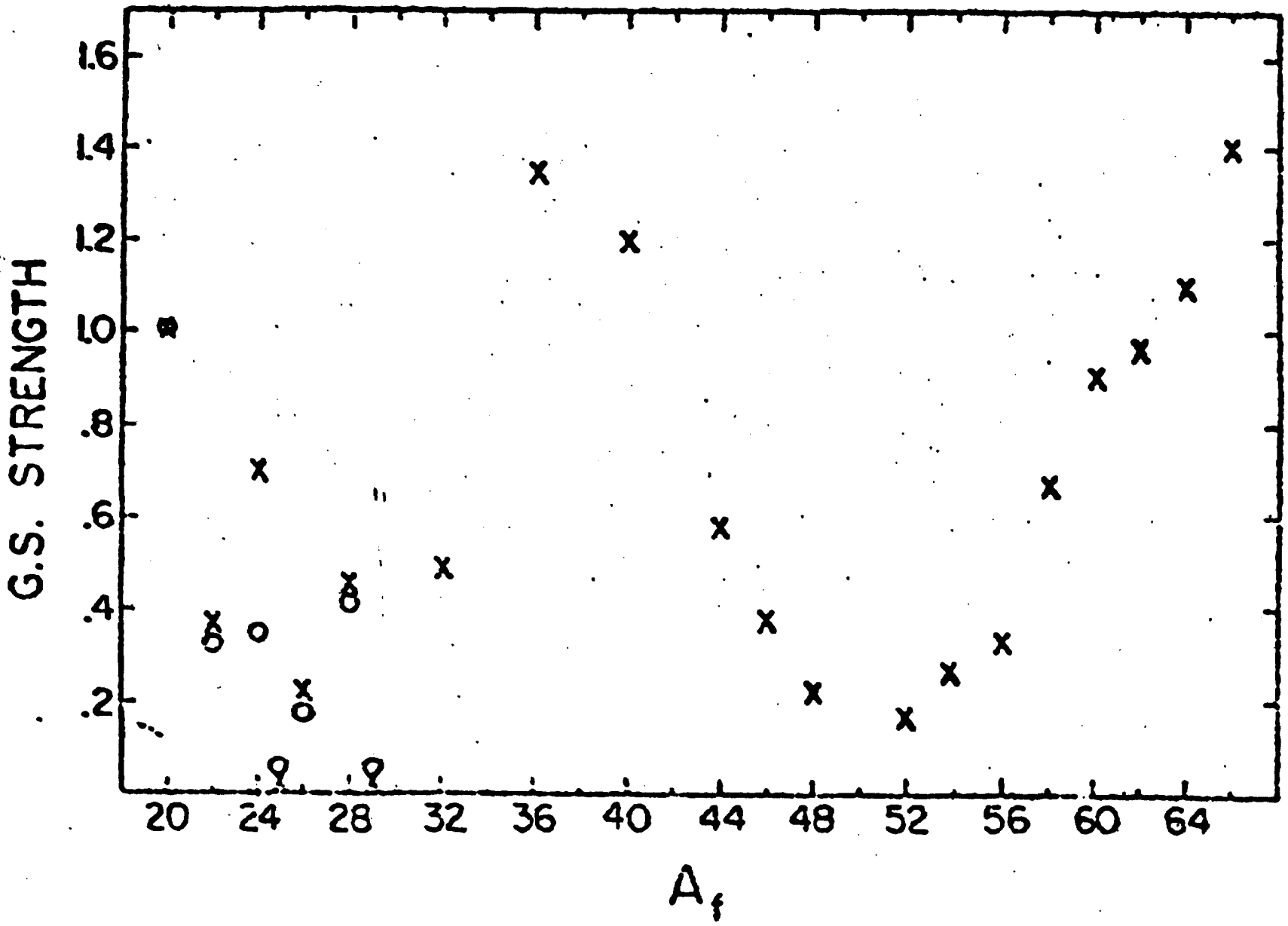

FIG. 19

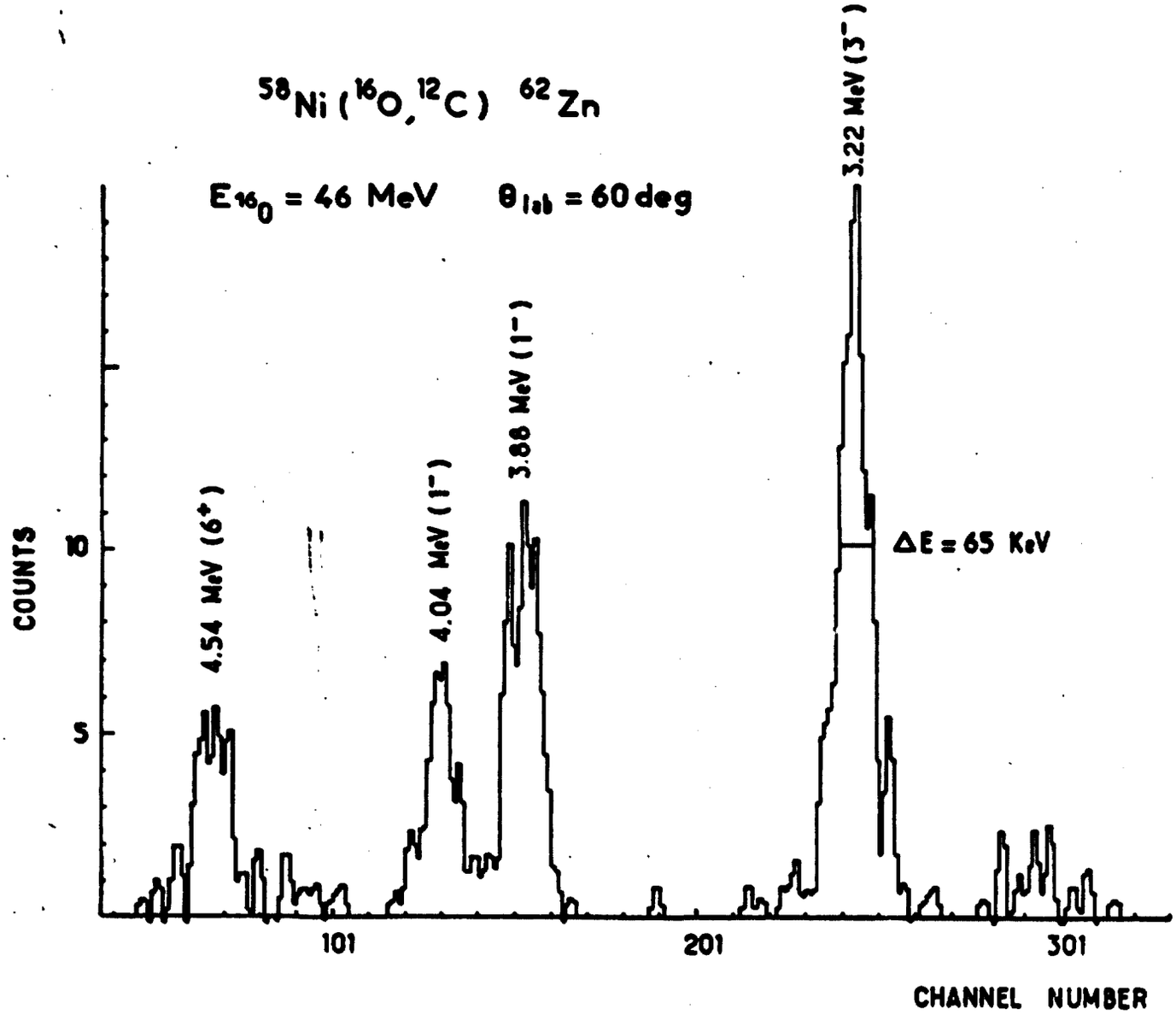
$^{58}Ni\,(^{16}O,^{12}C)\,^{62}Zn$
$E_{^{16}O}$ = 46 MeV
θ_{lab} = 60 deg
3.22 MeV (3⁻)
3.88 MeV (1⁻)
4.04 MeV (1⁻)
4.54 MeV (6⁺)
ΔE = 65 KeV
COUNTS
10
5
101
201
301
CHANNEL NUMBER

Fig.20

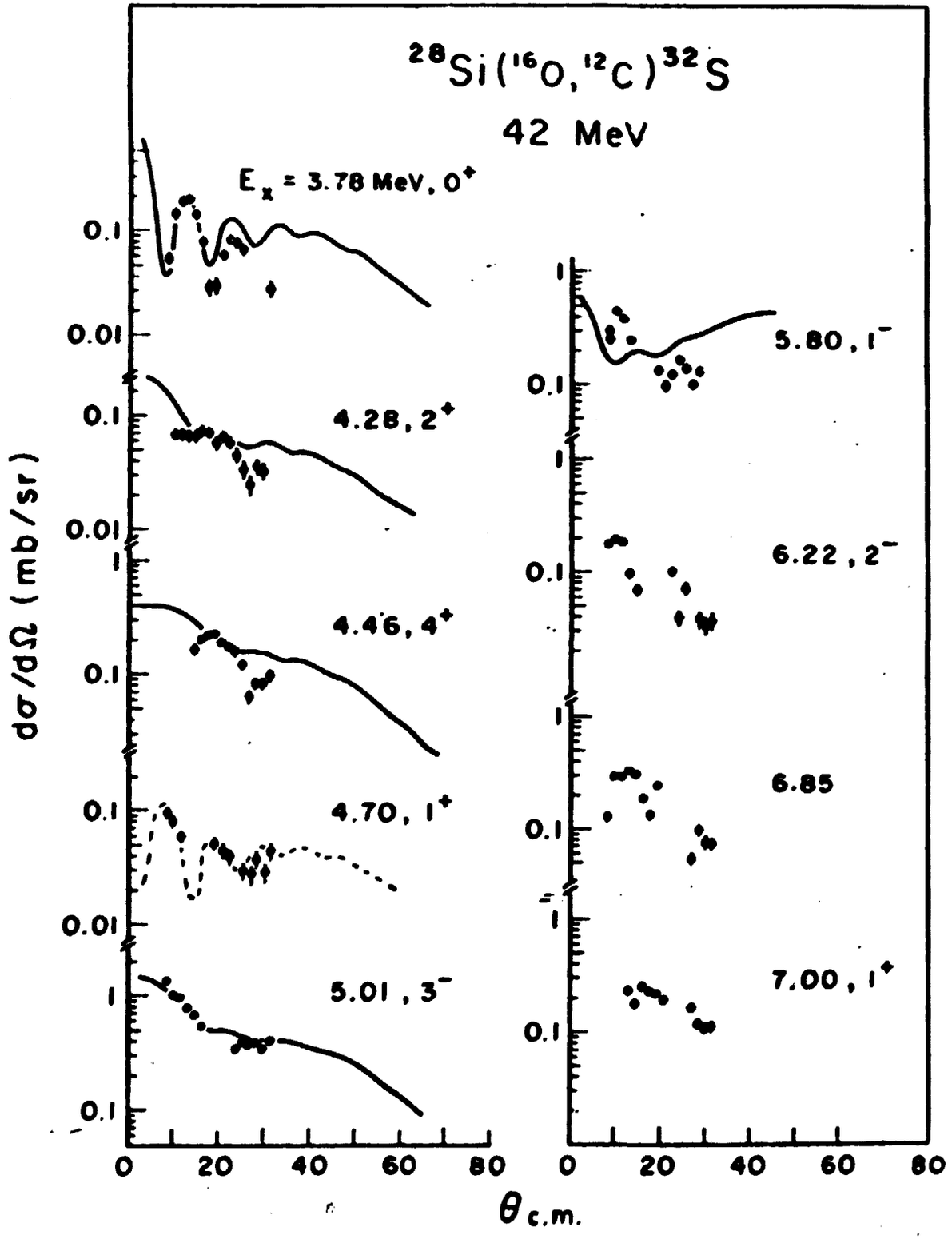
$^{28}Si(^{16}O,^{12}C)^{32}S$
42 MeV
E_x = 3.78 MeV, 0$^+$
4.28, 2$^+$
4.46, 4$^+$
4.70, 1$^+$
5.01, 3$^-$
5.80, 1$^-$
6.22, 2$^-$
6.85
7.00, 1$^+$
dσ/dΩ (mb/sr)
θ c.m.
0
20
40
60
80
0.1
0.01
1

Fig.21

TABLE I

Reactions	E_{lab}	Autors	References
^{72,74,76}Ge(^{16}O,^{14}C)^{74,76,78}Se	56 MeV	M.E. Cobern et al. M.-C. Lemaire et al. T. Tamura et al. T. Udagawa et al.	[29] [24] Phys. Lett. 51B (1974) 116. Phys. Lett. 57B (1975) 135.
^{64}Ni(^{16}O,^{14}C)^{66}Zn	56 MeV	M.C. Mermaz et al.	[33]
^{116}Sn(^{16}O,^{14}C)^{118}Te	64 MeV	M. Conjeaud et al.	[34]
^{26}Mg(^{16}O,^{14}C)^{28}Si	45 MeV	B. Sorensen	[35]
^{62}Ni(^{12}C,^{10}Be)^{64}Zn	48 MeV	A. Greiner	Thesis, Orsay (1976).
^{100}Mo(^{12}C,^{10}Be)^{102}Ru	48 MeV	M.C. Mermaz et al.	[33]
^{186}W(^{12}C,^{10}Be)^{188}Os	70 MeV		Phys. Lett. 55B (1975) 289.
^{120}Sn(^{18}O,^{16}O)^{122}Sn	99 MeV	D.K. Scott et al.	Phys. Rev. Lett. 34 (1975) 895.
^{122}Sn(^{16}O,^{18}O)^{120}Sn	104 MeV	R.S. Ascuitto et al. Glendenning	Phys. Lett. 47B (1973) 332.
		N.K. Glendenning and Wolschin	Phys. Rev. Lett. 34 (1975) 1642.
^{74}Ge(^{18}O,^{16}O)^{76}Ge	75 MeV	P.D. Bond et al.	Phys. Rev. to be published.
^{76}Ge(^{16}O,^{18}O)^{74}Ge	77,56 MeV	M.-C. Lemaire and K.S. Low	Phys. Rev. to be published.
^{148}Sm(^{18}O,^{16}O)^{150}Sm		B. Sorensen	Phys. Lett. 66B (1977) 119.
^{150}Sm(^{16}O,^{18}O)^{148}Sm	100 MeV		
^{144}Nd(^{12}C,^{14}C)^{142}Nd	78 MeV	K. Yagi et al.	Phys. Rev. Lett. 34 (1975) 96.
^{186}W(^{12}C,^{14}C)^{184}W	70 MeV	K.A. Erb et al.	Phys. Rev. Lett. 33 (1974) 1102.
^{154}Sm(^{12}C,^{14}C)^{152}Sm	65 MeV	D.L. Hanson et al.	Nucl. Phys. A269 (1976) 520.
^{182}W(^{12}C,^{14}C)^{180}W	70 MeV	D.L. Hanson et al.	Nucl. Phys. A269 (1976) 520.
^{124}Te(^{12}C,^{14}C)^{122}Te	70 MeV	R.J. Ascuitto et al.	Nucl. Phys. A273 (1976) 230.

TABLE II

Reaction	E_{MeV}	$R = \sigma_{exp}/\sigma_{theory}$			References
$^{64}Ni(^{16}O, ^{14}C)^{66}Zn$	56	g.s., 0^+	1.04 MeV, 2^+	2.83 MeV, 3^-	
DWBA		27	75	224	Mermaz et al. [33]
CCBA		35[a]	35	35	
$^{100}Mo(^{12}C, ^{10}Be)^{102}Ru$	48	g.s., 0^+	0.475 MeV, 2^+	2.0 MeV, 3^-	
DWBA		47	873	289	
CCBA $0^+ - 2^+$, $0^+ - 3^-$		28[b]	28	28	Mermaz et al. [33]
CCBA 0^+, 2^+, 3^-		58	36	20	
$^{116}Sn(^{16}O, ^{14}C)^{118}Te$	64	g.s., 0^+	0.61 MeV, 2^+		
DWBA		1	8		Conjeaud et al. [34]
CCBA		1	2.8		

:gin here »

TABLE III

$(N\ C^2S,\ C^2S_2)_{E_{xc},\ J^\pi}/(N\ C^2S,\ C^2S_2)_{g-s}$

	E_{xc}	J^π	Theory	$(^6Li,d)^a$	$(^{16}O,^{12}C)^b$
$^{24}Mg \rightarrow {}^{28}Si$	0.0	0^+	1	1	1
	1.78	2^+	0.21	0.22	0.20
	4.98	0^+	0.70		
	6.69	0^+	1	1	
	6.9	4^+			0.41
	E_{xc}	J^π		$(^6Li,d)^c$	$(^{16}O,^{12}C)^d$
$^{58}Ni \rightarrow {}^{62}Zn$	0.0	0^+		1	1
	0.95	2^+		0.48	0.48

a) Ref.[40] c) H. Gutbrod et al., Phys. Rev. Lett. 29 (1972) et réf.[47]
b) Ref.[49] d) Ref.[47]

TABLE IV

Transition	peak $d\sigma/d\Omega$ (μb/sr)	γ_α^2(keV) $(^{16}O,^{12}C)$	α-decay
$^{204}Pb+\alpha \rightleftarrows {}^{208}Po$	0.05±0.03	0.39±.23	0.33±.0002
$^{207}Pb+\alpha \rightleftarrows {}^{211}Po$	0.16±0.06	0.20±.075	0.064±.0046
$^{208}Pb+\alpha \rightleftarrows {}^{212}Po$	0.75±0.16	1.4 ±.17	1.3 ±.0088
$^{208}Pb+\alpha \rightleftarrows {}^{212}Po^*(0.727)$	1.75±0.26	0.84±.072	0.89 ±.27
$^{209}Bi+\alpha \rightleftarrows {}^{213}At$	0.70±0.17	1.1 ±.27	1.5 ±.27